Laser Processing of Emerging Nanomaterials for Optoelectronics and Photocatalysis

Anna Lipovka, Aura Garcia, Elena Abyzova, Maxim Fatkullin, Ziyang Song, Yuxiang Li, Ranran Wang, Raul D. Rodriguez,* and Evgeniya Sheremet*

Optoelectronics and photocatalysis are two rapidly developing photonic fields that are revolutionizing green energy, medicine, communications, and robotics. To advance these areas and explore new applications, there is a need for new materials and technologies that enable fast, scalable, and customizable production of high-performing optoelectronics, including the future development of flexible devices. This review is focused on the strategies to synthesize novel, not fully explored materials and/or enhance their properties using the powerful method of laser processing. The discussion includes the laser treatment of MXenes, Metal-Organic Frameworks, and perovskites, materials' advantages in terms of structural, electronic, and optical properties, and the role of different laser-based techniques in boosting their performance. Additionally, there is a demonstration of the existing and potential applications of these three materials and their combinations, especially in optoelectronics and photocatalytic platforms. This review aims to provide a comprehensive understanding of the current state-of-the-art in this field to help researchers identify opportunities and challenges in laser processing of emerging nanomaterials for optoelectronics and photocatalysis.

1. Introduction

The materials that hold the potential to be used in optical devices and, at the same time, possess mechanical flexibility have gained significant interest in recent years due to their future use in photodetectors, photodiodes, or transparent conductors, which can be folded into different shapes. Such devices would promote progress in touch screens, solar cells, displays, wearable electronics, and smart sensors.[1–4] Conventionally used in optoelectronics silicon, gallium arsenide, indium phosphide, indium tin oxide (ITO), and fluorinated tin oxide (FTO) proved to be highly efficient for photodiodes, light-emitting diodes (LEDs), and liquid-crystal displays (LCDs).[5,6] However, they fail to meet the demands of flexible devices due to their rigid nature, fragility, and relatively high cost. This has driven a shift toward modern low-dimensional materials, which may offer improved functionality to devices thanks to their extraordinary properties revealed at the nanoscale.[7]

MXenes, Metal-Organic Frameworks (MOFs), and perovskites are among the most promising emerging low-dimensional materials for these objectives, as proposed in recent studies by Bartolomeo et al. and Kumbhakar et al.[8,9] Each material demonstrates notable characteristics, including high surface area, tunable electronic structure, and versatile structural properties. As a result, they hold significant potential for a wide range of applications in optoelectronics and photocatalysis.[10] Individually, MXenes are famous for their high electrical conductivity, mechanical robustness, and adjustable optical transparency. They can absorb visible and near-infrared (NIR) light, which can enhance the efficiency of photodetectors. MOFs, in turn, are characterized by high porosity, large surface area, and tunable optical properties like refractive index or optical bandgap.[11] These features are useful for photocatalysis and potentially for light-emitting devices. Finally, perovskites (being able to be both bulk crystals and nanomaterials, depending on the synthesis route) have a high absorption coefficient and high electron mobility, which makes them critical for photovoltaics and photodetectors. In some cases, two of these materials are used jointly, which results in even better performance and opens new perspectives.

However, all this comes with the challenges behind the benefits. Generally, synthesizing nanomaterials with precise control over size, chemical composition, and shape is not simple, as different factors like temperature, pH, synthesis time, pressure, and so on may greatly contribute to the result.[12] Moreover, hardly avoidable impurities and defects could also affect the

A. Lipovka, A. Garcia, E. Abyzova, M. Fatkullin, R. D. Rodriguez, E. Sheremet
Tomsk Polytechnic University
Lenin ave. 30, Tomsk 634050, Russia
E-mail: raul@tpu.ru

Z. Song, Y. Li, R. Wang
The State Key Lab of High Performance Ceramics and Superfine Microstructure
Shanghai Institute of Ceramics
Chinese Academy of Sciences
Shanghai 200050, China
E-mail: wangranran@mail.sic.ac.cn

R. Wang
School of Chemistry and Materials Science
Hangzhou Institute for Advanced Study
University of Chinese Academy of Sciences
Hangzhou 310024, China

The ORCID identification number(s) for the author(s) of this article can be found under https://doi.org/10.1002/adom.202303194

DOI: 10.1002/adom.202303194

surface and reactivity. Finally, for all three materials, environmental factors often compromise the stability.[13] For instance, the implementation of MOF/MXene composite proposed by Khosroshahi et al.[14] already faced the issue of poor long-term performance. There are several approaches to improve the stability, as well as to increase the crystallinity, mechanical, structural, and electrical properties of these materials for specific applications. These routes include improved synthesis protocols, functionalization and post-functionalization strategies, surface passivation, and different types of processing.[15]

Laser irradiation is one of the most efficient and adjustable ways to create or process emerging nanomaterials to enhance their properties and stability in a controlled manner, as well as to facilitate their integration into different substrates.[16–18] Lasers have already been used to modify the whole range of nanomaterials from graphene to metal nanoparticles.[19,20] Furthermore, prior discussions have thoroughly explored the advantages of employing laser processing techniques on 2D nanomaterials to create electronic and optoelectronic devices.[17] An additional benefit of using lasers is patterning the materials or their selective removal with submicrometer resolution, even beyond the diffraction limit.[21] This allows new features and a precise design of devices, excluding complicated lithography approaches. For MXenes, MOFs, and perovskites, some laser-based techniques have already been applied recently. To maximize the impact of these experimental findings, it is necessary to systematize the research results. Such a summary will help material scientists, physicists, and chemists to identify which laser approaches are beneficial and applicable to future developments in flexible optoelectronics and photocatalytic platforms.[22–24]

In this review, we discuss these materials' optical, electronic, and mechanical properties, highlighting their importance in various applications. Additionally, we provide an in-depth analysis of existing processing techniques aimed at improving the properties of these materials, emphasizing the role of laser processing in advancing research in this field. To maintain the scope of this review, we deliberately exclude the discussion of other well-studied nanomaterials like graphene, as our primary objective is to shed light on the potential applications of the lesser-explored new emerging materials.

Section 2 overviews the key properties of MXenes, MOFs, and perovskites. We highlight their unique features, advantages, joint use, and current limitations and challenges to overcome.

In Section 3, we introduce and summarize the efficiency of the existing ways to process emerging nanomaterials to improve their properties and stability.

Section 4 is dedicated to various laser processing methods for the synthesis and modification of emerging nanomaterials. We examine the effect of different laser-based techniques on morphological, structural, and electronic properties, discussing the opportunities of each of the methods.

In Section 5, we discuss the application of the chosen laser-processed emerging materials in optoelectronics, focusing on what has been achieved by now and the challenges that need to be addressed to make these materials more applicable in the future. We summarize the latest findings and achievements in this area and identify the knowledge gaps for further research.

Section 6 is dedicated to the current achievements in the use of the chosen laser-processed materials in photocatalysis.

Overall, this review represents a guide on implementing lasers to improve the performance of MXenes, MOFs, and perovskites, especially for applications in optoelectronics and photocatalytic devices.

2. Emerging Nanomaterials and their Properties. Perspectives for the Use in Optoelectronics and Photocatalysis

To fully reveal the potential of MXenes, MOFs, and perovskites in optoelectronics and photo/photoelectrocatalysis, including the use in flexibles, it is crucial to understand their original physicochemical properties (particularly optical and electrical ones) and to ensure that these materials can be transferred onto flexible substrates or be directly synthesized on them. To comprehend the historical context, highlight current advancements, and have an idea on the prospects of all three materials in optoelectronics and photocatalysis, we made a timeline showing the evolution of the key developments and findings in this area (**Figure 1**). All three chosen low-dimensional materials share a common feature of being adjustable in terms of chemical composition, synthesis, and processing, which allows their specific and tunable characteristics. This section briefly discusses the basics, synthesis routes, and properties of MXenes, MOFs, and perovskites (**Figures 2–4**). We discuss their individual applications in optoelectronics and photocatalysis, as well as recent advancements in the use of their combinations. We also identify current issues in the field and outline future research prospects for these emerging nanomaterials in flexible devices.

Figure 1 illustrates that the current trends across all three materials are very similar: wearables, photocatalysis, optoelectronics, and enhanced efficiency and stability. The aims are coherent even though the materials were discovered in different decades and have distinct historical backgrounds and properties. Perovskites notably lead in reaching the commercial level, given that they were originally intended for optoelectronic applications. Figure 1 contains references to the following manuscripts: Yan et al.,[25] Gatou et al.,[26] Kojima et al.,[27] Li et al.,[28] Gogotsi et al.,[29] Gulati et al.,[30] Kumar et al.,[31] Park et al.,[32] Peng et al.[33] Wang et al.,[34] Deng et al.,[35] Lee et al.,[36] Agresti et al.,[37] Jiang et al.,[38] Levitt et al.,[39] Al-Ashouri et al.,[40] Yang et al.,[41] Hussain et al.,[42] Li et al.,[43] Aydin et al.[44]

2.1. MXenes

MXenes' rapid development started with the discovery of 2D titanium carbide (Ti_3C_2) in 2011.[45] The materials are described by a formula $M_{n+1}X_nT_x$, where M is a transition metal (such as Ti, Ta, V), X – carbon or nitrogen, and T_x^- surface termination groups (—OH, —O, or —F). In most cases, MXenes are synthesized through the chemical etching of the A component (the element of the IIIA or IVA group) from the MAX phase (Figure 2).[46] The choice of etching agent affects morphology, surface groups, and defects.[46] MXenes exhibit conductivity values ranging from dozens to several thousands of S cm^{-1}, comparable with metal oxides' conductivity, including ITO, conventionally used in flexible electronics ($10^2 – 10^4$ S cm^{-1}).[47] So far, the highest reported conductivity value of 2×10^4 S cm^{-1} was

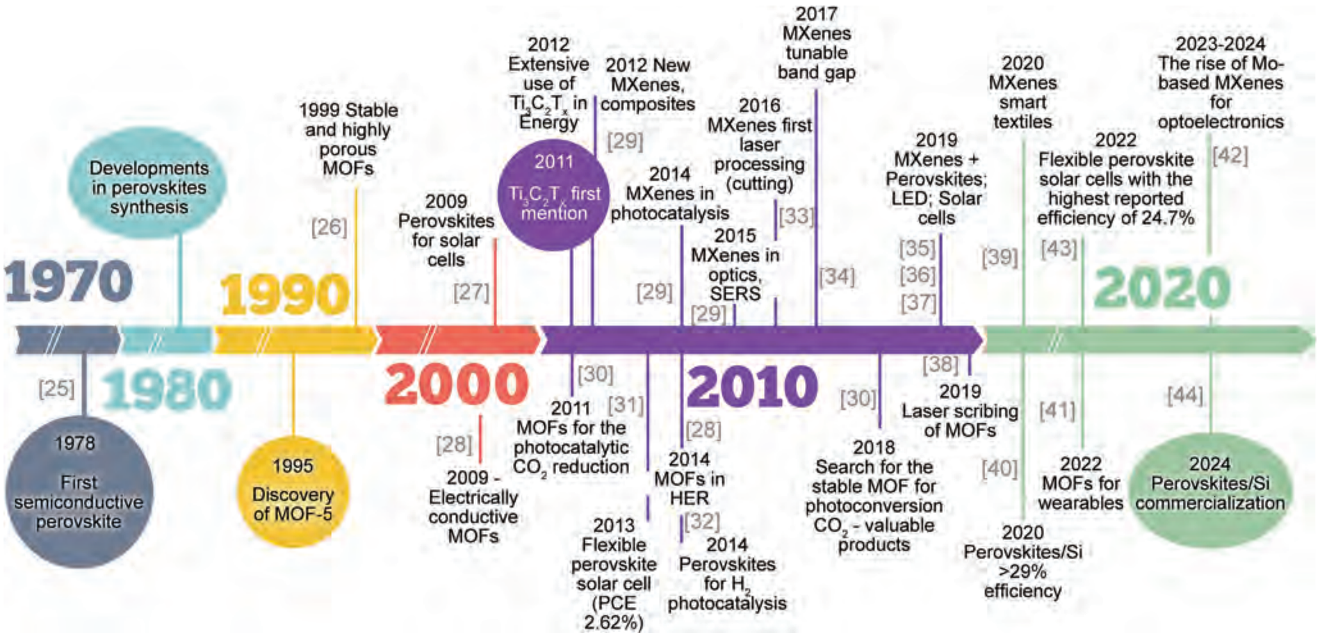

Figure 1. Timeline with the historical background and the key moments that defined the current research directions in the use of emerging materials in optoelectronics and photocatalysis.

achieved for $Ti_3C_2T_x$.[48] Also, depending on the material choice, MXenes conductivity type could vary. Most show metallic band structure, while some indicate bandgaps of 0.1 – 2 eV (Figure 2).[49] Importantly, these 2D materials are highly elastic due to the layered structure and weak van der Waals bonding between the layers, allowing for easy bending and deformation without losing structural integrity.

MXenes generally exhibit strong absorption in the ultraviolet (UV) and visible ranges while being transparent in the near-infrared (NIR) region. However, depending on the nature, they could exhibit plasmonic peaks covering the entire vis-NIR region and various colors in transmission (for thin films) and reflection (for multilayer films).[50] The tunable bandgap (Figure 2), high conductivity, and mechanical flexibility make MXenes highly promising for applications in optoelectronics and photodetectors.[51] So far, MXenes have been used as metamaterial plasmonic absorbers, surface-enhanced Raman scattering substrates,[52] transparent conductive electrodes in flexible displays,[46] and flexible conductors and interconnects for optoelectronic devices.[53] MXenes have shown high and quick photoresponse in photodetectors, indicating their suitability for use in optical communication systems and imaging sensors. All these opportunities together led to the development of a new field known as "MXetronics," which refers to the fabrication of fully MXene-based electronics.[49]

The common complications for MXenes lie in their engineering and deposition on substrates. There are several approaches to address these issues and enhance MXenes properties. For instance, an effective strategy is to dope or combine MXenes with other materials, as discussed in Section 2.4.[54,55] Furthermore, additional treatments and surface functionalization techniques, explored in Section 3, are also efficient in improving the applicability of MXenes further.

2.2. MOFs

MOFs are synthesized by the self-assembly of metal ions and organic ligands. The most commonly used ions are Zn_2^+, Cu_2^+, Ni_2^+, while organic ligands can range from simple carboxylic acid to more complex molecules (Figure 3). High porosity makes MOFs ideal for various applications, the most obvious of which are gas storage, catalysis, and drug delivery.[57,58] The high surface area, ranging from hundreds to thousands of m^2/g, generally not exceeding 10000 $m^2\ g^{-1}$[59,60] is one of the most important characteristic features of MOFs. It makes a larger interface for light absorption and emission to improve the device's efficiency. Other intriguing prospects of MOFs include the flexibility of electrical and optical properties reached by varying the chemical composition and multiple options of deposition on the substrates.

While most MOFs exhibit electrical insulating properties caused by the poor electron transfer between non-redox active metal centers and organic linkers, certain MOFs can be conductors or semiconductors. The introduction of electrical conductivity in MOFs is achieved by incorporating redox molecules, metallic species like Ni, Cu, Fe, or Co, or specific linkers, enabling conductivity values of up to a tenth S cm^{-1}.[61]

In terms of optical properties, MOFs exhibit light absorption, exciton generation, fluorescence, and luminescence. These characteristics vary depending on the interactions between the metal centers and the organic ligands chosen for synthesis, as well as the confinement of guest molecules within the pores.[62,63] The optical bandgap of MOFs spans from 1.0 to 5.5 eV (Figure 3). MOFs can efficiently absorb light in the UV–vis and NIR regions, rendering them valuable for applications in photocatalysis and solar energy conversion.[64] Additionally, MOFs can exhibit photochromism, enabling reversible alterations of their color or optical properties in response to light. This property opens up

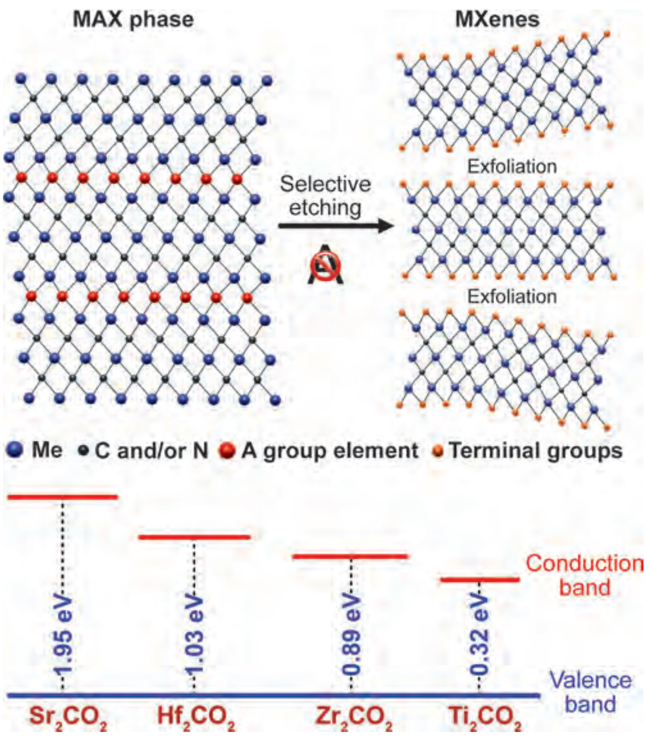

Figure 2. Schematic illustration of selective etching of the MAX phase and subsequent exfoliation to form MXenes, and the energy level diagrams with bandgap values for MXenes made of different transition metals. Summarized from the previously reported data.[56]

possibilities in data storage and sensing.[65] Chromophore networks within certain MOFs enable efficient light-harvesting arrays, replicating this capability for light-to-electrical conversion.[9] Recently there have been demonstrations of MOFs as flexible interconnects for optoelectronic devices,[66] including transparent conductors in flexible displays.[57,67–71]

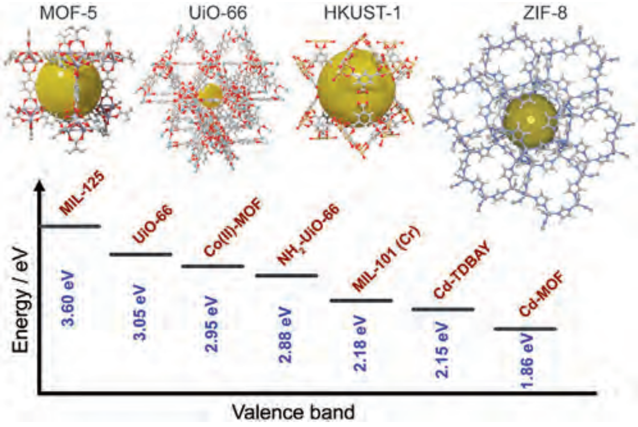

Figure 3. Schematic illustration of several MOFs with their pore accessibility indicated by yellow spheres, and schematic illustration of band diagrams with bandgaps of several widely used MOFs revealing differences in electronic properties crucial for various applications. Created following previously reported data.[72–74]

Despite the benefits of MOFs in optoelectronics, there are still several challenges that need to be addressed. For example, improving MOFs stability and surface modification is crucial, as well as developing new synthesis methods to improve reproducibility and control over the structure.

2.3. Perovskites

Perovskites are highly demanded materials for applications in advanced optics. Their crystal structure is typically described by the formula ABX_3, where A and B are two different cations, and X is an octahedron anion bonded to both cations. Similar to van der Waals materials, the properties of most perovskites could be tuned by going from the bulk materials to the nanoscale.[75] The versatility of perovskites lies in the ability to replace each component, facilitating the fine-tuning of properties tailored to specific applications.[76–78] This elemental variation offers an opportunity to precisely control the bandgap of perovskites. For example, in $BaZrO_3$ (E_g = 3.9 eV), substituting oxygen with sulfur to form $BaZrS_3$ reduces the bandgap to 1.7 eV.[79] Thus, the bandgap could be tuned through the entire visible range (Figure 4). Additionally, perovskites demonstrate high optical absorption (with an absorption coefficient in the range of 10^3–10^4 cm^{-1}), high electron mobility, efficient charge transport, high luminescence, and quantum yield.[80–82] Their advantages complement mechanical flexibility and solution processability.[78,83]

Over the past decade, a new class of perovskites, known as organic-inorganic hybrid perovskites (OIHP), has gained tremendous attention from scientists and the industry. Unlike standard perovskites, OIHPs consist of cations composed of both organic and inorganic species. In OIHPs, the organic cations (e.g., $CH_3NH_3^+$, $CH(NH_2)_2^+$, $CH_3CH_2NH_3^+$)[84,85] are denoted by the A component, while the B component represents a bivalent heavy metal cation. The anions are typically represented by halides. The reason these materials are getting so widespread and discussed further in this review is the long lifetime of photogenerated free charge carriers (≈µs), relatively low exciton binding energy, and high tolerance toward the defects.[75,86]

Besides these relatively new findings, the other developing area is the synthesis of perovskite quantum dots (PQDs), which are particularly important for photodetectors and optoelectronic synapses. PeQDs significantly amplify NIR light absorption through organic capping, achieving adjustable carrier transport to precisely modulate memory transition from short-term to long-term via optical stimulation.[87]

The properties mentioned above made perovskites highly attractive for application in flexible optoelectronics, particularly in the field of photovoltaics.[88] In fact, perovskites have already been successfully employed as active materials in flexible solar cells and light-emitting devices.[89] There are notable achievements in using metal halide perovskites (particularly lead-based ones) to fabricate flexible inorganic LEDs that can be integrated into optoelectronic systems with a power conversion efficiency (PCE) of 23.3%. Such LEDs exhibit exceptionally narrow emission linewidths, diverse sizes and structures, and the additional advantage of low-temperature synthesis.[3]

The stability of perovskites remains a significant challenge as they are susceptible to degradation over time, particularly due

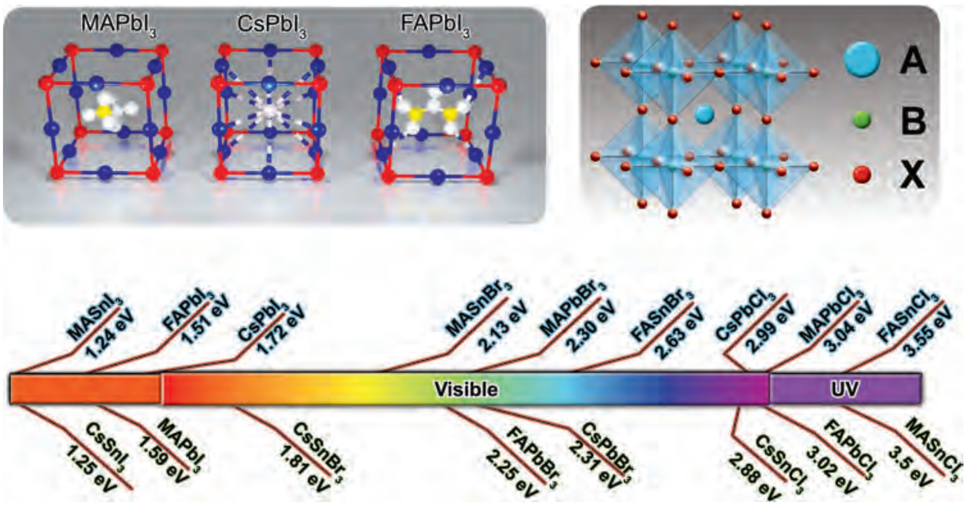

Figure 4. Schematic illustration of bandgap distribution across halide perovskites: Various halide perovskites and their corresponding bandgap energies, mapped against the electromagnetic spectrum regions they absorb: near-infrared (NIR), visible, and ultraviolet (UV). Accompanying structural representation illustrates the ABX_3 perovskite cubic crystalline structure and some representative forms of lead halide perovskites.[92]

to moisture and heat.[90] Another obstacle that has hindered the application of perovskites in flexible displays is the difficulty in achieving stable and pure red, green, and blue emission wavelengths at 650, 525, and 450 nm, respectively.[91] Strategies to improve these factors will promote the research on perovskites to a new level.

2.4. Combining MXenes, MOFs, and Perovskites for Optoelectronics

The joint use of emerging materials is inspiring. For example, combining high conductivity and transparency of MXenes with tunable optical properties of MOFs and perovskites could result in transparent conductors with improved optical properties. Similarly, combining MXenes with perovskites can lead to the development of flexible photodetectors with increased sensitivity and stability. Despite that these three materials were never used together, in this subsection we discuss the existing cases of combining two of them to get enhanced functionality.

2.4.1. MXenes + Perovskites

The introduction of MXenes to perovskite-based solar cells helped getting a higher PCE compared to using perovskites alone. This was achieved by the band alignment and work function (WF) reduction caused by dipole induction in the perovskites/MXenes interfaces.[37,93] In this sense, MXenes seem to be a perfect candidate for doping to create next-generation photovoltaic devices since different chemical compositions (in particular, a variety of termination groups) allow fine and precise tuning of device electronic properties.[37,93,94] Spontaneously organized OH/O termination with a ratio of 50/50 reduces work WF to 3.1 eV, while the ratio of 75/25 in MXenes itself gives WF of 1.9 eV, as shown by Agresti et al.[37] MXenes in solar cells build a bridge between the perovskite absorbing layer and electron transport layer (ETL) to suppress electron accumulation and align the growth of perovskite crystals (Wu et al.).[95] These features allowed for the improvement of the performance of SnO_2-MXene-based perovskite solar cells by 15% compared to SnO_2-based perovskite.

Besides the application in optoelectronics, MXenes-perovskite composites revealed themselves as highly efficient photocatalysts. Since MXenes could exhibit metallic properties, and perovskites are semiconductors, the appearance of the Schottky barrier is typical for such a material combination. This, in turn, leads to controlled adsorption and molecule activation, enhancing catalytic activity.[96] $Cs_2AgBiBr_6/Ti_3C_2T_x$ Schottky heterostructures were utilized for the remarkable catalytic organic dye degradation, being ≈4.7 times more efficient than pristine $Cs_2AgBiBr_6$. This enhancement is attributed to the enlarged interfacial contact area and favorable Fermi level alignment, promoting enhanced charge transfer capabilities, efficient separation, and suppressed electron-hole recombination.[96,97] Also, in a recent study by Saravanakumar et al.,[98] Ti_3C_2 MXene quantum dots (MQDs) were introduced into perovskite-based Z-scheme heterostructure as charge-transport bridges to form In_2S_3/MQDs/$SmFeO_3$. Such configuration demonstrated photocatalytic degradation efficiency of 98% for 4-chlorophenol. This work identified the optimal MQD concentrations for the highest performance.[98]

2.4.2. MOFs + Perovskites

The combination of perovskites with MOFs has also been investigated recently. MOFs were used to encapsulate organic PeQDs to improve their thermal stability and photostability for long-term performing LEDs.[99] This improvement was achieved by controlling the pore sizes in MOFs and incorporating the PeQDs into the pores. Several works confirmed that this approach could be used to protect perovskite nanocrystals.[100] Another strategy for utilizing MOFs in perovskite-based photovoltaic devices is to use them for the fabrication of more efficient ETLs, which have enhanced carrier mobility and low recombination rate compared to the conventional ones. Vinogradov et al.[101] combined MIL-125 MOF with the conventionally used TiO_2 using a single-step hydrothermal synthesis to achieve a highly stable depleted monolithic perovskite/MOF@TiO_2 with enhanced PCE compared to the one with bare TiO_2. This approach was also applied to increase the PCE efficiency in other research works.[102,103]

Similar to MXenes, MOFs were also utilized for interface engineering in perovskite solar cells. MOFs offer the potential for controlled growth of perovskite layers and the improved contact between the perovskites and the ETL.[104] Certain MOFs, like ZIF-8, not only serve as an interface engineering material but also act as an additional absorbing layer, contributing to an enhancement in overall device performance.[105] The efficiency of MOFs made them a popular choice to combine with other materials, not only for optoelectronics, but also for sensors, electrodes for hydrogen evolution reactions (HER), and energy storage devices, as it was demonstrated in the case of the joint use with MXenes.[106–108]

The MOFs guest-host interactions were also utilized to embed PQDs in their pores. Wu et al.[109] employed Fe-porphyrin-based MOF PCN-221(Fe_x) to encapsulate $MAPbI_3$ to protect it from degradation. Utilizing the sequential deposition method, the authors achieved a record-high total yield of 1559 μmol g^{-1} for photocatalytic CO_2 reduction. Another strategy to enhance the photocatalytic activity of perovskites by implementing MOF is harnessing the exceptionally high surface area of MOFs to provide active sites for molecule adsorption. This approach was used for $KNbO_3$ in the N_2 reduction. While bare perovskite exhibits a low surface area of 0.68 – 3.9 m^2 g^{-1}, insufficient for efficient photocatalytic reduction, the introduction of TMI-5 MOF (surface area 591 m^2 g^{-1}) resulted in a surface area increase to 172 m^2 g^{-1} ($KNbO_3$@TMU-5). This combination not only improved the photocatalytic transformation of N_2 to NH_3 from 20.5 (for bare $KNbO_3$) to 39.9 μmol L^{-1} h^{-1} g^{-1} (for $KNbO_3$@TMU-5), but also enhanced the stability and reusability of the photocatalyst. After the fifth cycle of use, the reaction efficiency remained high at 37.9 μmol L^{-1} h^{-1} g^{-1}. The formation of composite with MOF additionally suppressed electron-hole recombination due to internal charge transfer between $KNbO_3$ and TMU-5, as well as a higher negative charge density on Nb sites (Chamack et al.).[110]

2.4.3. MXenes + MOFs

Taking into account the properties of MXenes and MOFs, it is absolutely justified that there are no research works utilizing their combination in optoelectronics. However, this pairing has been found to be applicable in photocatalysis. $Ti_3C_2T_X$ MXenes played a significant role in modulating the properties of Ti_3C_2-based MIL-125-NH_2 nanohybrids synthesized via a single-step solvothermal process. This unique combination led to a 1.65 times higher yield in H_2O_2 photocatalytic production and 11.5 times higher photocatalytic degradation of tetracycline hydrochloride under visible light ($\lambda > 420$ nm) compared to bare MIL-125-NH_2. The performance improvement was attributed to dual-heterojunction formation, enhancing carrier density and facilitating interfacial charge transfer and separation.[111] In another study by Shahriyari et al.,[112] solvothermal-grown Zn-MOF crystals were deposited on $Ti_3C_2T_X$ MXene nanosheets to fabricate highly efficient and durable photocatalysts. This composite had a highly porous structure with a high specific surface area, promoting a rapid charge transfer along with the reduced recombination rate for photo-generated carriers. Photo-excited electrons transfer through MXene and MOF bands accelerated radical production for photocatalytic degradation of dyes. Ultimately, the MXene/Zn-MOF photocatalysts demonstrated a photodegradation efficiency of 62% for methylene blue and 35% for direct red 31.[112]

In conclusion, the combination of MXenes, MOFs, and perovskites has the potential to overcome limitations in existing materials and to contribute to new materials with enhanced performance and functionality. Further research in this field is necessary to fully realize the potential of such combinations, and to bring innovative flexible optoelectronics and photocatalytic platforms to the market. In optoelectronics, we expect future works to focus on chasing higher efficiency and developing flexible devices. As for photocatalysis, the critical moment is the mechanism. Among various approaches, S-scheme heterojunctions are the freshest approach to boosting photocatalysts efficiency and reducing fabrication costs. In this configuration, two semiconductors with differing Fermi levels and WFs are brought into contact. Electrons migrate from the semiconductor with the lower WF toward the one with the higher, creating an interfacial layer with accumulated electrons, generating internal electric fields. This system is pushing itself to reach an equilibrium by aligning Fermi levels (band bending). Upon irradiation, weak charge carriers recombine via Coulombic attraction, while strong electrons and holes participate in redox events.[97,113] S-scheme heterojunctions have emerged as a solid alternative to Z-scheme heterojunctions, and their development is expected in the future.

Section 2 provided an overview of the unique properties exhibited by MXenes, MOFs, and perovskites, including their high surface area, exceptional electronic and optical properties, and mechanical flexibility. These properties make them promising candidates for a wide range of applications, particularly in optoelectronics and photocatalysis, with a perspective in flexible devices. However, these materials also have inherent drawbacks that need to be addressed either through upgrading the synthesis protocols or through the use of specific processing techniques. The main challenges are connected to the materials' stability and the ways to enhance functionality. To address this, researchers are exploring innovative methods such as tuning synthesis parameters, introducing dopants, and implementing surface modifications, which are discussed in the next section.

3. Conventional Processing of MXenes, MOFs, and Perovskites to Increase their Performance: Challenges and Strategies

To expand the implementation of emerging materials and make their use more sustainable, several processing techniques can be used. Processing methods are crucial in addressing several limitations, including preventing degradation, morphology and structure control, interface engineering, performance enhancement, and scalability.

This section provides an overview of the ways to address these issues. Laser treatment, which is the focus of this review, is not discussed here since it will be examined later extensively.

3.1. Processing of MXenes

Processing offers a solution to enhance the electrical conductivity of MXenes. For example, Urbankovski et al.[114] used ammoniation to convert Mo_2CT_x and V_2CT_x from carbide to nitride MXenes at a temperature of 600 °C. This process replaced carbon atoms with nitrogen ones via ammonia decomposition, resulting in nitride MXenes that exhibit metallic conductivity instead of the original semiconducting carbide MXenes. A similar outcome can be obtained by introducing sulfur or phosphorus.[115] Alternatively, the conductivity can be tuned by simple thermal treatment, which can be carried out in an inert atmosphere or under a vacuum. Thermal annealing reduces the number of surface termination groups, particularly fluorine, which changes the band structure and increases electrical conductivity.[116] Thermal treatment is one of the most used approaches to control or modify surface termination of MXenes.[116–118]

Besides conductivity, processing could also enhance the mechanical properties and stability of MXenes. Liu et al.[119] presented a biomimetic nanocomposite between MXenes and PEDOT:PSS produced by vacuum-assisted filtration. The sample showed a six times higher tensile stress than the initial $Ti_3C_2T_x$ MXene had. Stability of MXenes toward degradation was achieved by Wu et al.[120] using hydrothermal carbonization of glucose, adsorbed on the $Ti_3C_2T_x$ MXene at 160 °C. This resulted in the formation of a carbon layer (carbon nanoplating), which protected MXenes from degradation not only at ambient conditions but also during hydrothermal reactions and high-temperature thermal annealing.

Processing routes play a crucial role in addressing the limitations of MXenes and enabling their development into high-performance materials for a wide range of applications, which was summarized in the recent review articles by Tang et al., Persson et al., Khazaei et al., and Jiang et al.[115,121–123] The further development in this direction will accelerate the commercialization of MXenes and their widespread use in industry.[124,125]

3.2. Processing of MOFs

The techniques to process MOFs aim to enhance their structural, mechanical, and chemical stability. For instance, the moisture stability of MOF-5 crystals was increased by adding surfactants during the drying process, which resulted in a hydrophobic surface.[126] Moreover, activation processes are frequently employed to eliminate solvent molecules and excess linkers, thus achieving permanent porosity, large accessible surface area, and enhanced stability. There are several methods for activating MOFs, including freeze-drying, chemical treatment, solvent exchange using low-surface tension solvents, and more conventional heating and vacuum techniques.[127]

It is widespread to functionalize the pores of MOFs to exploit their ability to interact with guest molecules. Sol-gel processing is one of the most used methods for these purposes. A sol (colloidal suspension) transforms into a gel-like material, which can be used as a precursor for coating or doping MOFs with guest molecules. Another functionalization was proposed by Sanil et al.,[128] who utilized aminopropylisooctyl polyhedral oligomeric silsesquioxane (O-POSS) to selectively functionalize HKUST-1 MOFs, resulting in increased hydrophobicity and moisture stability. The authors showed that this approach is universal by functionalizing MOF-74 and MIL-100(Fe) in the same way to gain hydrophobicity with the introduction of O-POSS.

Another objective of processing MOFs is to enhance their electrical conductivity, which is a must-have property for the straightforward application of MOFs in sensors, optoelectronics, and (photo)catalysis. Several review articles are dedicated to this issue,[61,71,129] all concur on several promising ways to turn MOFs conductive. These methods include composite formation with conductive nanomaterials, post-processing, impregnation with guest molecules, or combination with conductive polymers.

These findings have practical implications for a broad range of MOF applications, such as gas separation, catalysis, and energy storage.[130–132] Recent advances in processing techniques have enabled the development of MOFs with improved stability and selectivity.[69,133]

3.3. Processing of Perovskites

One of the primary obstacles to perovskites' wide use is their inherent instability, which results in degradation under environmental conditions such as exposure to moisture, heat, and light. There are several ways to avoid this, such as changing chemical composition or using processing like thin film encapsulation,[134] utilizing additives,[135] and employing anti-solvent engineering.[136]

Similar to MXenes and MOFs, thermal annealing is one of the most common ways to improve the stability and homogeneity of perovskites.[137] Pool et al.[138] demonstrated that conventional annealing using a heating plate is not the only way to make such a process. Instead, they performed radiative thermal annealing (RTA) of $FAPbI_3$ spin-coated film using a NIR lamp. It was shown that the best condition to form the perovskite phase is heating at 170 °C for 40 s using this RTA. The other alternative to conventional heating could be even room temperature processing to achieve perovskite crystallization.[139]

Surface treatment is another promising approach for perovskite processing. For example, the incorporation of organic molecules, such as alkylamines or carboxylic acids, was used to passivate the surface of perovskite solar cells and prevent undesirable chemical reactions.[140] The addition of different tin halides forms a protective layer on the surface of perovskites, which helps prevent moisture and other environmental factors from affecting the film. Among the proposed additives (SnI_2, $SnBr_2$, $SnCl_2$, SnF_2), tin chloride ($SnCl_2$) is the most efficient in improving perovskite stability at ambient conditions. In fact, $SnCl_2$ demonstrated a remarkable 6.7-fold increase in stability compared to pristine B-γ $CsSnI_3$, as evaluated by monitoring the absorbance at 500 nm.[141]

Finally, doping is one of the most widespread ways to improve the stability of perovskites. The literature explores various cations for this purpose, including group 14, transition metals, alkaline earth metals, trivalent cations, and polymers.[142–146] All the mentioned routes also proved to manipulate the optical properties of perovskites through a band alignment or changing the bandgap.[147]

While processing perovskites is a complex and challenging task, realizing their full potential in photovoltaics, LEDs, and sensors is essential.[148–150]

Despite the considerable advancements in processing MXenes, MOFs, and perovskites, there is still plenty of room to develop new methods to address their challenges.[151] In this regard, laser processing offers several advantages over conventional processing techniques, as extensively discussed in the next section.[152]

4. Laser Processing of Emerging Nanomaterials: Impact on their Properties and Performance

The use of lasers in the synthesis and modification of nanomaterials has been actively developing in recent years due to their efficiency, precision, and versatility.[153] Laser-assisted methods offer several advantages over other methods. These include the ability to achieve spatial selectivity down to the diffraction limit and, in some cases, even beyond, facilitate nanostructuring, enable local thinning or increasing the porosity, provide precise control over the shape and size, and manipulate material properties with minimum fabrication steps (often without the need of special environmental conditions). Recently, some of the laser-assisted approaches have been implemented for the synthesis and modification of MXenes, MOFs, and perovskites.[17,18,24]

Laser irradiation is different from other light sources in that it has spatial and temporal coherence, is monochromatic, has low divergence, and is highly intense. The basics of laser processing rely on the excitation of electrons from the equilibrium state by the absorption of photons by atoms or molecules.[154] Once the irradiation is absorbed, the light intensity with the depth decays according to Beer-Lambert's law:

$$I(z) = I_0 e^{-\alpha z} \tag{1}$$

where α is the absorption coefficient, and I_0 – is the initial intensity of the beam just reaching the surface. The optical absorption depth is often defined as $1/\alpha$, indicating the value in which the intensity decreases to $1/e$ of the original value when considering linear optics. Other effects take place while using short pulses or materials with a nonlinear refraction index, like self-focusing, defocusing, and soliton propagation.[155] Laser-induced matter modification can be achieved through a variety of mechanisms, which can be broadly classified into three categories: photothermal effects, photochemical effects, and nonlinear optical effects (**Figure 5**). The probability of non-linear absorption increases with shorter pulses since the pulse width is less than the relaxation time. Figure 5 illustrates that non-thermal carrier-carrier Coulomb interactions start at the fs timescale. Hot electrons can undergo cooling by the emission of phonons. Relaxation to optical phonons typically takes from fractions to several ps, while to acoustic phonons, from several to dozen ps. Beyond this threshold, thermal processes appear. Thermal diffusion arises from electron-lattice interactions and phonon coupling.[156]

In the photothermal theory, the laser energy is absorbed by free electrons in the material. The excess energy of the excited electrons is rapidly transferred to the lattice, causing the rise of the temperature, and is rapidly dissipated through electron-electron scattering. The energy is further transferred to the surrounding environment through electron-phonon coupling.[155,157,158] In photochemical processes, lasers can initiate or accelerate chemical reactions in the material, which is sufficient to break bonds directly (photo-decomposition), leading to changes in the material's chemical structure and new properties.[159,160] In nonlinear optics, the interaction of laser irradiation with the material produces new photons with different frequencies and/or directions. Various effects, including self-focusing, self-phase modulation, and harmonic generation, can be used to create new materials or to modify the properties of existing ones.[161]

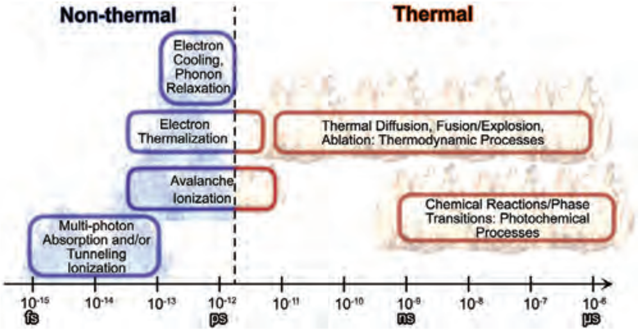

Figure 5. Timeline illustrating the processes behind laser treatment. Summarized using the reported data.[156,160]

Considering the variety of mechanisms, it could be difficult to identify or predict the exact one for the particular case since a whole set of parameters and material properties needs to be taken into account, affecting the outcome, such as local heating, melting, ablation, or photoinduced chemical reactions.

The quality and properties of nanomaterials synthesized or processed using lasers rely on such key laser parameters as wavelength, power density, pulse duration and frequency, beam profile, pulse energy, and scanning speed.[21,152,153,162,163] For instance, in the case of continuous wave (CW) or nanosecond pulses, the absorption happens due to single-photon interactions, following the classical heat transfer model, while for the shorter femtosecond and picosecond pulses, there is an optical breakdown and multiphoton absorption, which results in a decreased depth, and an additional opportunity for non-thermal transitions to take occur.[155] For ultrashort pulses, the laser width is significantly shorter than the electron cooling time, which allows to neglect energy transfer from electrons to the lattice. Consequently, electrons reach high temperatures while the lattice remains relatively cool. This implies that for longer ns pulses, the whole treated nanoparticle will be heated, while for fs and ps, only the surface lattice is heated, which protects the shape and size of nanoparticles. This phenomenon could potentially preserve the shape and size of processed nanoparticles. Simulations showed that using the fs laser the maximum laser penetration depth is ≈40 nm.[156]

When we aim to understand the mechanisms behind the processing of new materials, lasers are often treated as black boxes, which limits the advancement of fundamental science. This section discusses the methods employed in the synthesis and properties manipulation of emerging nanomaterials. The literature data regarding processing types, crucial experimental details, and results are summarized in **Table** 1 and are discussed in the text below.

CW-nanosecond lasers, where the thermal effect is dominant, are often used when the possible thermal damage of the surrounding area is not critical, and the short pulses are used for more sensitive and localized processing.[164]

Briefly, the most used lasers for processing emerging materials are CO_2 (CW/µs), Nd:YAG (ns), diode (CW), fs, and ps laser with unspecified source (likely Ti:sapphire or fiber lasers). CO_2 and ns lasers are typically favored for annealing and scribing. The ultrashort pulses are a more preferable choice for materials ablation because of the minimal heat-affected zone and high spatial resolution, which results in minimal material damage in the applications with high precision.

It is important to note that the terminology used to describe different laser processes significantly varies from report to report. This variation arises from the author's choice to highlight different aspects or propose their own more relevant terms. To simplify understanding, we have classified laser-assisted strategies into several approaches based on the underlying processes. These approaches are divided into:

- annealing and scribing as its special case (Sections 4.1 and 4.2),
- ablation and cutting as its special case (Sections 4.3 and 4.4),
- other less widespread methods (Section 4.5).

To ensure clarity, we provide explicit definitions of each process at the beginning of every subsection, even though, in some cases, it is not obvious how to separate the laser effects as there might be their combination.

4.1. Laser Annealing

Laser annealing is a conventional technique for modifying the surface properties of different materials by rapidly heating the material to high temperatures for a short time. Annealing can significantly alter the material's crystallinity, morphology, or electronic properties without removing it from the surface.[208] Unlike thermal annealing, laser annealing often does not require special environmental conditions or a vacuum to prevent oxidation or contamination due to its high speed and localized area.[209] Additionally, the laser effect is localized and could be used to treat specific parts of the material with free-form patterning. Laser annealing is applicable for the processing of temperature-sensitive substrates, which is not possible with thermal annealing and thus has a limitation in working with low melting point materials. Annealing occurs at a specific threshold depending on several factors, such as laser wavelength, power density, pulse duration, and the material to be processed.[210] During annealing, laser radiation is absorbed by the material's surface, raising its temperature. Temperature control is realized through the choice of pulse length and laser intensity to achieve localized melting. The heat diffuses according to the thermal gradient, and further cooling down results in recrystallization. This is the physical process behind it, which is leading to alterations in the crystal lattice structure, roughness, size and shape of the particles, and defect concentration. All this together enhances the crystallinity and changes morphology of the material (**Figure** 6a).[211] Low thermal dissipation is needed to achieve the high temperature gradient and heating rate characteristic for laser annealing, and the ability to modify properties with nanometer resolution and impact only desired areas, leaving the rest of the material intact.[212] However, heat dissipation along with processing conditions will also define the cooling rate, which increases with power decrease.[213] The cooling rate is the highest right after the laser is off, with a tendency to slow down with time. Depending on the aim and conditions, a laser might also facilitate the integration of dopants into the material or induce surface carbonization, which will introduce or increase electrical conductivity. Laser annealing has been reported to synthesize or modify the properties of MOFs and perovskites, making them suitable for energy, sensing, and optoelectronic applications.

4.1.1. Laser Annealing of MOFs

An illustrative example of laser annealing applied to MOFs is reported by Tang et al.,[165] who systematically investigated laser-induced annealing of 12 different MOFs on 8 conductive substrates using CO_2 laser (4.8 W). Laser annealing was used to carbonize MOFs to form transition-metal-based core-shell composites, where the high temperature induced by the laser in MIL-101(Fe)/NF caused the decomposition of the organic ligands forming carbon and reducing Fe ions to Fe metal NPs. In the presence of air, Fe is oxidized to form stable Fe_3O_4. The carbon atoms rearrange themselves to form a core-shell structure around the metal particles for their further use in electrochemical water splitting. Compared to thermal annealing, the use of laser irradiation helped to reduce the processing time, avoid the use of an inert atmosphere, and prevent aggregation while maintaining a high yield. This strategy is promising not only for water splitting but also for the fabrication of supercapacitors and sensors (Figure 6b).[165] Meanwhile, another study suggested synthesizing Cu-BTC (also known as HKUST-1) by immersing an oxidized copper substrate in a solution of trimesic acid and irradiating it with a nanosecond Nd:YAG laser at a wavelength of 532 nm. The acid decomposes into H^+ and BTC ions, while the reaction of H^+ with copper hydroxide on the substrate generates Cu^{2+}. Laser energy induces the generation of Cu^{2+}, OH hydroxyl radicals, and highly transient temperatures. These temperature changes induce chemical reactions between Cu^{2+} and BTC ions. As a result, a MOF film with a thickness of ≈10 µm is formed on the copper substrate. The process behind this is explained with the following reactions:

$$\mathrm{Cu(OH)_2} + h\nu \rightarrow \mathrm{Cu^{2+}} + 2\mathrm{OH^-} \quad (2)$$

$$2\mathrm{H_3BTC} \rightarrow 6\mathrm{H^+} + 2\mathrm{BTC^{3-}} \quad (3)$$

$$3\mathrm{Cu(OH)_2} + 6\mathrm{H^+} \rightarrow 3\mathrm{Cu^{2+}} + 6\mathrm{H_2O} \quad (4)$$

$$3\mathrm{Cu^{2+}} + 2\mathrm{BTC} \rightarrow \mathrm{Cu_3(BTC)_2} \quad (5)$$

These investigations pave the way for photothermal laser processing to be used to synthesize other MOFs for energy materials and devices.[166]

To date, those are the only works that specifically discuss laser annealing of MOFs. Most commonly, the laser is used to form specific shapes, which is more related to laser scribing.

Table 1. Laser processing approaches.

Laser annealing						
Laser source (pulse width)	Wavelength, laser power	Emerging material	Product	Application	Addressing issues	References
CO_2 (N/A)	10.6 µm, 4.8 W	MOF	LIA-MOF/ Substrate	water splitting	avoiding particle aggregation, increasing the yield, and reducing the time consumption	Tang et al., 2021[165]
Nd:YAG (ns)	532 nm, N/A	Cu DMF, BTC	HKUST-1	synthesis	synthesizing solutions	Lee et al., 2022[166]
Nd:YAG (ns)	1064 nm, N/A	perovskites	$MAPbI_3$	crystallization	annealing time, crystallization improvement	Malyokov et al, 2018[167]
Diode (CW)	405 nm, 450 nm, and 660 nm, 150 mW	perovskites	$MAPbI_3$ and $(CsPbI_3)_{0.05}$ $(FAPbI_3)_{0.95}$-$(MAPbBr_3)_{0.05}$ films	PSCs	controlling the crystallization of perovskite films	You et al., 2020[168]
N/A	N/A	MXene/ BP	MXene/BP hybrid film	MSC	expanding the interlayers of MXene sheets; accelerating ion diffusion	Zhang et al., 2021[169]
CO_2 (µs)	10.6 µm, ≈ 5 W	MXene/Au/paper	thick MXene coplanar electrodes	MSC	first time MXene-on-paper	Kurra el at., 2016[170]
N/A	N/A, 4.8 W	MXene	MXene-based films	MSC	preventing damage due to external deformation and improving conductivity	Li et al., 2020[171]

Laser scribing – *patterning, writing, carving*						
Laser source (pulse width)	Wavelength, laser power	Emerging material	Product	Application	Addressing issues	References
KrF (N/A)	248 nm, N/A	MXene/ Fe_3O_4	MXene/Fe_3O_4/ MXene electrode	MSC	reducing oxidation of MXene	Li et al., 2021[172]
N/A (ns)	1064 nm, 3.8 W	MXene	MXene film	SC	alleviating the restacking of MXene film	Tang et al., 2020[173]
CO_2 (N/A)	N/A, 1 W	MXene /GO	MXene/rGO nanocomposite	pressure sensor	pressure-sensing performances	Zhao et al., 2021[174]
CO_2 (µs)	10.6 mm, 3.6 W	PI/MXenes	LIG/MXenes nanocomposite	gas sensing	increasing active sites and gas adsorption	Zhang et al., 2023[175]
CO_2 (N/A)	10.6 µm, N/A	MXene	MXene-reinforced hierarchical nanofibers	e-tattoos	converting CNFs from PVDF	Sharifuzzaman et al., 2021[176]
CO_2 (N/A)	10.6 µm, N/A	MXene/ MFNFs	nanohybrid patch (TiO_2@LCNFs-based HBeT)	soft wearable electronics	producing CNFs	Sharifuzzaman et al., 2023[177]
CO_2 (N/A)	10.6 µm, from 2.4 to 4.2 W	MOF	core–shell structured composite	MSC	producing MOF-derived carbon nanomaterials	Zhang et al., 2021[178]
CO_2 (N/A)	10.6 µm, 9 – 10 W	MOF/ porous graphene	LIMDG	MSC	developing functional materials	Basu et al., 2016[179]

(*Continued*)

Table 1. (Continued)

Laser scribing – *patterning, writing, carving*

Laser source (pulse width)	Wavelength, laser power	Emerging material	Product	Application	Addressing issues	References
Diode (N/A)	405 nm, 450 – 950 mW	MOF/PET	LIG	photothermal heater	developing functional materials from waste	Kogolev et al. 2023[180]
CO_2 (N/A)	10.6 µm, from 0.6 to 3.6 W	MXene/ MOF	LC MXene/MOF nanocomposite	TENGs	developing intermediate layer for TENGs	Salauddin et al., 2022[181]
CO_2 (N/A)	9.2--10.8 µm, 12 W max.	MOF	MOF-5, HKUST-1, ZIF-8, UIO-66 and Zn-JAST-1	synthesis	synthesizing various MOFs without chemical functionalization of substrates	Hirai et al., 2017[182]
N/A (fs)	532 nm, N/A	Tb(BTC)·G	LMOFs	synthesis	synthesizing and patterning simultaneously	Liu et al., 2021[183]
YLP (ns)	1064 nm, from 1.5 to 4.5 W	MOFs as precursor	MNPs (Fe, Co, Ni, Cu, Zn, Cd, In, Pb, and Bi)	synthesis of MNPs	synthesizing and patterning MNPs simultaneously	Jiang et al., 2019[38]
YLP (ns)	1064 nm, from 1 to 10 W	MOFs as precursor	metal alloy nanoparticles	synthesis of metal alloy nanoparticles	synthesizing metal alloy nanoparticles	Ma et al., 2020[184]
Diode, CW	405 nm, from 150 mW to 1500 mW	MOFs	hierarchical porous MOFs	synthesis	removing photosensitive linkers selectively	Wang et al., 2020[185]
Ti:sapphire (fs)	800 nm, N/A	PQDs	3D PQDs	photonic devices	exploring new functionalities and applications in optoelectronics	Huang et al., 2020[186]
Nd:YAG (ns)	1064, 532, and 355 nm, N/A	perovskite	perovskite film	photodetector array	modifying the bandgap	Xu et al., 2022[187]
Diode (CW)	410 nm, 100 mW	inorganic–organic Perovskites	non-contact micro/nano patterning	LEDs	precise patterning; efficient PL at ≈518 nm	Kanaujia and Vijaya, 2016[188]

Laser ablation – *etching*

Laser source (pulse width)	Wavelength, laser power	Emerging material	Product	Application	Addressing issues	References
N/A (fs)	1030 nm, ≈ 1.1 mW	MXene	MXene film	MSC	manufacturing solutions	Li et al., 2020[189]
N/A (fs)	520 nm, N/A	MXene	MXene/TiO_2 membrane with aligned micro-channels	Lithium-metal batteries	regulating lithium-deposition	Xiong et al., 2020[190]
N/A	N/A	MXene/ MoS_2	free-standing MXene-MoS_2 film	MSC	manufacturing solutions	Chen et al. 2019[191]
CO_2 (N/A)	10.6 µm, from 1 to 8 W	metallo- hydrogel	TMCs (MoC_x, WC_x, and CoC_x)	MSC, energy harvesting	developing ultrathin TMCs	Zang et al., 2019[192]
Ti: sapphire (fs)	N/A	MXene, GO	MQD/LRGO	transparent SCs	preparing QD composites in one step	Yuan et al., 2022[24]
Nd:YVO_4 (N/A)	532 nm, from 200 to 300 mW	ZnO film	ZIF-8 films	from micro-fluidics to renewable energy systems	enabling the precise and facile fabrication of MOF patterning	Bo et al., 2022[193]

(*Continued*)

Table 1. (Continued)

Laser ablation – *etching*						
Laser source (pulse width)	Wavelength, laser power	Emerging material	Product	Application	Addressing issues	References
Nd:YAG (ns)	1064 nm, 20W	MOF, brass support	ZIF-8 membrane	gas separation	producing MOF micromembranes	Navarro et al., 2014[194]
Nd:YAG (N/A)	1064 nm, N/A	MOF	ZIF-67	Synthesis	synthesizing solutions	Ribeiro et al., 2019[195]
Nd:YAG (ns)	N/A	Cu in DMF/H_2O	HKUST-1	Synthesis	synthesizing solutions	Campello et al., 2015[196]
Nd:YAG (ns)	1064 nm, N/A	bismut, DMF, MeOH, BTC	bismuth-based MOF	Synthesis	synthesizing solutions	Ataei et al., 2020[197]
Nd:YVO_4 (ns)	355, 532, and 1064 nm, from 10 mW to 1 W	Perovskites	absorber patterning	PSCs	selectively removing the perovskite absorber layer	Turan et al., 2017[198]
1. N/A (ps) 2. N/A (ns)	1. 1064 nm, N/A 2. 532 nm, N/A	Perovskites	absorber patterning	PSCs	selectively removing the perovskite absorber layer	Schultz et al., 2020[199]
various: Nd:YVO_4, fibre laser, Ti:Al_2O_3, KrF (various: ns, ps, fs)	various:from 248 nm to 2.5 µm, N/A	Perovskites	absorber patterning	PSCs	upscaling to large area solar modules	Bayer et al., 2017[200]
Laser ablation – *cutting*						
N/A (fs)	N/A	MXene	MXene ribbons	SC	restacking of MXene film	Zheng., 2022[201]
UV (N/A)	N/A	MXene, Ni	MXene/Ni film	MSC	manufacturing solutions	Wang et al., 2019[202]
Other strategies						
Laser source (pulse width)	Wavelength, laser power	Emerging material	Product	Application	Addressing issues	References
Yb:YAG (N/A)	1070 nm, 20.6 W	MXene	MXene-reinforced composite by L-PBF	aerospace, automotive, and biomedical engineering	reinforcing MMCs	Zhou et al., 2022[203]
Nd:YAG (ns)	1064 nm, N/A	MOF and LMNPs	liquid metal nanolayer-linked MOF by laser shock evaporation	synthesis	synthesizing solutions	An et al., 2021[204]
YLP (ns)	1064 nm, 10 W	MOF	noble metal catalysts (Pt, Au, Rh, Ru) conjoined on CeO_2	synthesis	synthesizing uniform catalysts	Guo et al., 2020[205]
CO_2 (N/A)	10.6 µm, 24 W	Sulfur-impregnated MOFs	metal sulfide nanoparticles	synthesis, SC	synthesizing solutions	Van Lam et al., 2022[206]
N/A (fs)	516 nm, 30 mW	PEG-modified ZIF-8 powder	pure ZIF-8 films	synthesis	synthesizing solutions	Fischer et al., 2017[207]

Note: BP, black phosphorus; CNFs, carbon nanofibers; CW, continuous wave; DMF, dimethylformamide; GO, graphene oxide; KrF, krypton fluoride; L-PBF, laser powder bed fusion; LC, Laser-carbonized; LIA-MOF, laser-induced annealing MOF; LIG, laser-induced graphene; LIMDG, laser-induced MOF-derived graphene; LMNPs, liquid metal nanoparticles; LMOFs, luminescent metal-organic frameworks; MeOH, methanol; MFNFs, fluoropolymers nanofibers; MMCs, metal matrix composites; TiO_2@LCNFs-based HBeT, titanium dioxide laser-carbonaceous nanofibrous-based hybrid bioelectronic textile; MNPs, metallic nanoparticles; MOF-TFs, metal-organic framework thin films; MQD/LRGO, MXene quantum dots/graphene composite; MSCs, micro-supercapacitor; Nd:YAG, Neodymium-doped Yttrium Aluminum Garnet; Nd:YVO_4, Neodymium-doped Yttrium Orthovanadate; N/A, not available; PEG, polyethylene glycol; PI, polyimide; PL, photoluminescence; PQDs, perovskite quantum dots; PSCs, perovskite solar cells; PVDF, poly(vinylidene fluoride); rGO, reduced graphene oxide; SC, supercapacitor; TENGs, triboelectric nano- generators; TMOS, transitional metal oxides; TMCs, transition metal carbides; TiO_2@LCNFs-based HBeT, titanium dioxide laser-carbonaceous nanofibrous-based hybrid bioelectronic textile; UV, ultraviolet; YLP, Ytterbium nanosecond pulse fiber laser; Tb(BTC)·G, luminescent MOF based on terbium; BTC, tricarboxylic acid.

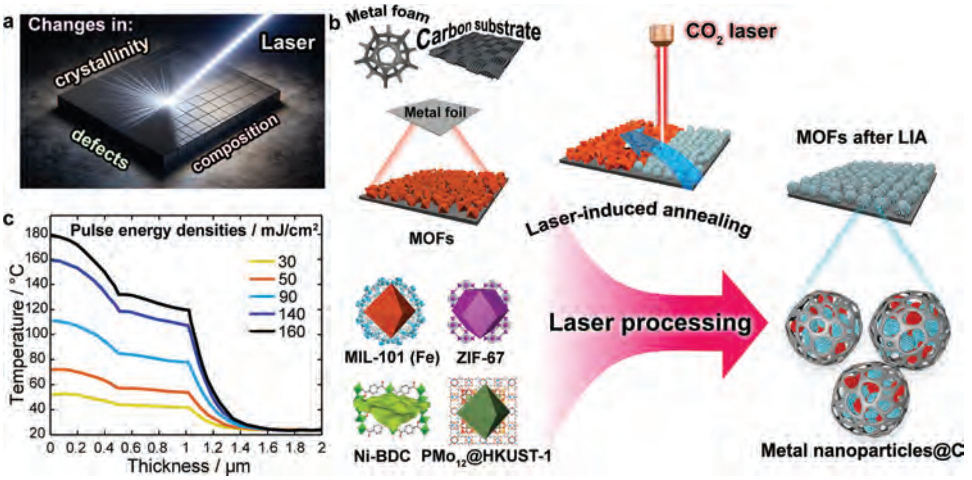

Figure 6. Laser annealing. a) Schematic illustration of the process. b) Laser annealing of different types of MOFs. Reproduced with permission.[165] Copyright 2021, Wiley-VCH. c) Simulation of the temperature reached on the surface of the perovskite precursor on the substrate. Drawn following the report.[167]

4.1.2. Laser Annealing of Perovskites

Conventional thermal annealing faces challenges in precisely controlling the crystallization of perovskites and is time and energy-consuming, which makes perovskites incompatible with low-temperature and fast fabrication required for certain devices. Laser annealing may overcome these limitations and enable the mass-production of perovskite solar cells with improved efficiency. For instance, 1064 nm pulsed laser irradiation was used to induce photothermal crystallization of a thin $MAPbI_3$ film. The selection of the appropriate wavelength is critical and should depend on the absorption characteristics of the perovskite precursor so that high-absorption regions are avoided to prevent ablation. In the study of Malyokov et al., the temperatures reached by laser processing are comparable to those attained during thermal annealing (Figure 6c). The temperature range of 120–160 °C was found to be optimal, resulting in a grain size of 490 nm and uniform morphology.[167] Different laser wavelengths (405, 450, and 660 nm) were applied in continuous mode to improve the crystallinity of perovskites. Among these, the 450 nm was the most effective for laser-induced crystallization. This is due to the induced local heating (≈100 °C) occurring only at the center of the spot, where the temperature gradient acts as the driving force for the formation of large grains. In this case, laser processing, unlike conventional thermal treatment, provides local and rapid heating (43 °C s^{-1}), leading to large grains formation, which is impossible to reach using an oven.[168] All the other examples of laser annealing of perovskites are directly dedicated to the fabrication of optoelectronic devices and are discussed in Section 5.

4.2. Laser Scribing

Laser annealing is effective in locally changing material properties through the photothermal effect, while laser scribing utilizes the same effect with a focus on creating specific patterns within emerging materials rather than modifying the entire surface (**Figure 7a**). Laser-induced fabrication of predefined shapes is also referred to as patterning, writing, or carving in various works. Numerous laser options are available for scribing, ranging from near UV to IR, meaning that physically there could be a combination of photothermal and photochemical effects, or one of the mechanisms dominating.[214–216] As the material absorbs the laser irradiation, thermal expansion or shrinkage occurs, creating stress and causing hollow grooves or trenches on the surface.[217] Laser exposure can cause structural changes in nanomaterials through photochemical and photothermal effects such as photolysis and redox processes, modifying the chemical composition and structure. The exact mechanism of laser scribing depends on laser parameters, material properties, and the substrate's optical and mechanical properties, as well as the desired pattern geometry.[218] It is crucial to note that excessive laser energy can result in rapid phase changes leading to ablation, discussed in subsection 4.3.

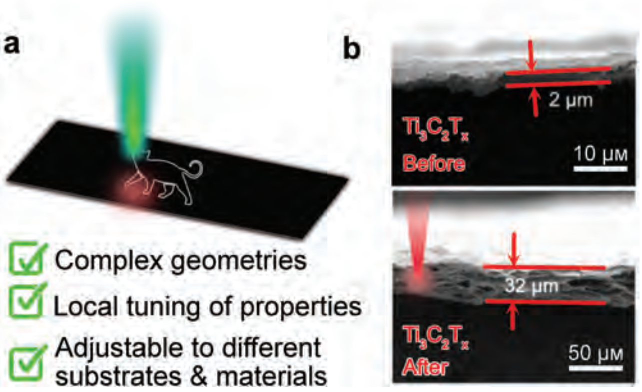

Figure 7. Laser scribing of MXenes. a) Schematic illustration of the process. b) Morphology change introduced by laser scribing. Adapted with permission.[173] Copyright 2020, Elsevier.

4.2.1. Laser Scribing of MXenes

Nowadays, laser scribing with different sources is a widespread approach. The most often used lasers remain CO_2 or Nd:YAG, especially for the fabrication of microsupercapacitors (MSCs) and other energy-related applications. Studies have shown that laser scribing of MXenes using CO_2 lasers and less powerful engravers significantly enhances the performance of MSCs by increasing porosity.[169–171,219] However, the heat generated during the process may also cause partial oxidation of MXenes on the pattern edges, which in turn can adversely affect the device's performance.[170] Li et al.[172] proposed to form a dense and uniform Fe_3O_4 layer between two MXene layers using laser crystallization, creating a barrier that prevents oxygen from reaching the Fe_3O_4 layer, thus reducing oxidation and improving electrode stability. The resulting MXene/Fe_3O_4/MXene sandwich-like structure showed a specific capacitance of 46.4 mF cm^{-2} and impressive cycling stability. Except for oxidation, the issue that MXenes could face in MSCs is the hindered ion transport caused by the restacking of 2D layers. However, laser processing can address this problem as well. Ultrafast laser writing helped to open the restacked layers and form a mesoporous structure of $Ti_3C_2T_x$ (Figure 7b).[173] Under the influence of the laser, the -OH surface groups and adsorbed water molecules were removed from the surface of $Ti_3C_2T_x$ nanosheets. In contrast, the appearance of bubbles on the surface and a significant increase of the thickness from 2 to 32 µm evidenced the gasification, as was previously shown for the case of laser reduction of graphene oxide (GO).[220]

Mentioning laser patterning of GO, in recent works, MXenes have often been combined with graphene-based materials for SCs.[221,222] Laser scribing of MXenes/graphene has proven to be useful not only for energy-related applications but also for sensors, ranging from simple pressure sensors to more complex wearable platforms. For instance, Zhao et al.[175] reported a pressure sensor fabricated by patterning a MXene/GO film on a flexible polydimethylsiloxane (PDMS) substrate using a CO_2 laser. The hybrid film on PDMS was first heated in an oven to 90 °C, and then the laser was used to reduce GO and pattern lamellar network-like cross-linked MXene/rGO structures.[174] A very similar system was used to achieve LIG/MXenes nanocomposites on a PDMS substrate fabricated using two-step laser processing.[175]

Going further to wearable electronics, laser scribing was applied to develop MXene-reinforced hierarchical nanofibers for e-tattoos. Sharifuzzaman et al.[176] utilized the laser carbonization (LC) of MXene-poly(vinylidene fluoride) nanofibers to improve conductivity (up to 4 Ω sq^{-1}), as well as mechanical strength and flexibility, which make them ideal for use in wearable devices. Later, the same group used the LC technique to create porous laser-carbonaceous nanofibers (LCNFs). This method overcomes the limitations of traditional thermal processing by providing greater control over carbonization conditions, which ensures consistent conversion and enables scalable production. It was shown that laser power and speed affect the structure and carbonization efficiency. The implementation of laser on several steps (carbonization itself and cutting) in this research allowed the development of highly electrically conductive (15.6 Ω sq^{-1}) and porous $Ti_3C_2T_x$-derived soft nanohybrid patch (TiO_2@LCNFs), which was further used in bioelectronic textile (TiO_2@LCNFs-based HBeT). The presence of T_x during the laser irradiation gives the high thermal activity of Ti in $Ti_3C_2T_x$ to form crystalline TiO_2 in the desired areas.[177]

4.2.2. Laser Scribing of MOFs

The spatially confined tuning of properties of already fabricated MOFs through laser scribing was discussed in several works and is getting more widespread to get MOF derivatives.[223] It is well known that laser patterning can greatly increase surface area without the need to heat the whole surface, which typically involves maintaining temperatures above 1000 °C for several hours. This effect is widely used for graphene, its derivatives, and metal nanoparticle processing.[224,225] Moreover, laser scribing enables the fine-tuning of pore sizes, which effectively enhances sorption properties. As a result, to benefit from such a modification, most of the patterned MOFs are primarily used to fabricate MSCs. However, since these emerging materials are mostly insulating or poorly conducting (as discussed in Section 2.2), improving their electrical conductivity poses a significant challenge. This factor is rarely explicitly addressed in research papers, but it affects specific capacitance, which is crucial for energy applications.

Laser scribing can be done on both rigid and flexible substrates. For instance, Zhang et al.[178] made a direct patterning of drop-casted MOF films on a quartz substrate using a CO_2 laser to obtain laser-induced MOF-derived carbon. Under the laser's instant influence, it is possible to achieve local temperatures as high as 2000 °C. The laser-induced carbonization was replicated for six different MOFs with various metal ions (including Zn, Co, Cu, Al, Fe, and Ni). According to XRD analysis, the laser power played the most crucial role in the result. While values less than 4 W resulted in full carbonization, the higher powers led to carbon oxidation to CO_2 in the form of gas and ablation. The best product in terms of the mesoporous structure formation and electrochemical capacitance was achieved on MOF-199@ZIF-67, which was later used in MSCs fabrication.[178] The CO_2 laser pyrolytic carbonization technique was extended to flexible substrates to create a porous laser-induced MOF-derived graphene on kapton, a material commonly used in flexible electronics. The significant increase in porosity was caused by the laser-induced temperature gradient across the entire thickness of the sample. The resulting MSC device not only exhibited stable performance but also demonstrated remarkable flexibility, withstanding bending up to 150 degrees.[179] A recent study by Kogolev et al.[180] demonstrated direct laser scribing for carbonization of UiO-66, resulting in increased porosity and electrical conductivity (with a sheet resistance down to 10.4 ± 3.1 Ω sq^{-1}). Notably, such laser patterning also improved the stability of MOFs, as evidenced by constant sheet resistance values even after an abrasion test. What sets this work apart is that the authors grew MOFs on a hydrolyzed waste PET substrate via a solvothermal synthesis route and then processed it with a 405 nm microsecond pulse laser, resulting in a more environmentally friendly fabrication cycle.[180]

As highlighted in subsection 2.4, the combination of emerging materials may lead to significant benefits in developing new electronic devices, and laser scribing enables precise tuning of the properties of MXene-MOF composites. Processing of this combination may result in improved electrical conductiv-

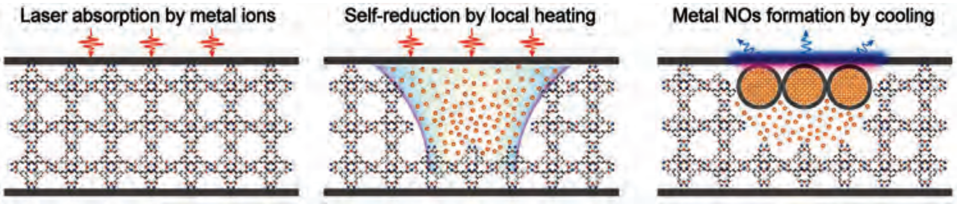

Figure 8. Laser scribing of MOFs. The processes behind nano-LaMP. Reprinted with permission.[38] Copyright 2019, American Chemical Society.

ity, surface roughness, and light absorption. Salauddin et al.[181] demonstrated these advantages by utilizing laser-carbonized MXene/ZiF-67 nanocomposite layers in triboelectric nanogenerators (TENGs), leading to higher output voltage and current. The porous structure of the nanocomposite layer, with its high density of charges, increases the surface potential and allows for longer retention of surface charges. Furthermore, the nanocomposite layer enhances light absorption and scattering in TENGs. Finally, the electrical properties of TENGs are further enhanced through increased conductivity and capacitance of the nanocomposite layer.[181]

Uniform heating and precise positioning of MOF crystals are critical factors not only for patterning but also for MOFs synthesis and future implementation in devices. Traditionally, bottom-up and top-down approaches are utilized to create MOFs in targeted locations. However, both of these approaches have limitations, as different techniques are only compatible with specific MOF types and reaction conditions. Therefore, they are not universal. Laser-based MOFs synthesis might be a more practical tool for precisely controlling heating spots. Hirai et al.[182] demonstrated the potential of laser synthesis of MOFs using infrared (IR) laser writing. This method utilizes a laser with a wavelength of 9.2–10.8 µm and a maximum power of 12 W to selectively heat MOFs precursors and induce their self-assembly into MOF crystals. The technique allowed the fabrication of various MOFs (MOF-5, HKUST-1, ZIF-8, UIO-66, and Zn-JAST-1) with precise control over size and position and was compatible with a wide range of MOF precursors and substrates without the need of chemical functionalization.[182] This work demonstrates that laser scribing offers greater flexibility in designing and synthesizing MOFs for specific applications than conventional methods. Additionally, the control over heating spots can lead to the formation of MOFs with improved crystallinity and morphology, which in turn can enhance the performance of MOF-based devices. In situ crystallization was shown for the synthesis and patterning of a luminescent MOF based on terbium Tb(BTC)·G with a wavelength in the visible range (532 nm). The high concentration of energy within the spot volume of less than 1 µm^3 allowed the nucleation and growth of Tb(BTC)·G. Improved crystallinity resulted in enhanced luminescence, represented by two peaks: 1) the Tb ions within the framework, which produced an antenna effect and amplified the luminescence intensity, and 2) the organic groups in the Tb(BTC)·G linkers absorb photons and transfer this energy to the Tb ions within the framework, resulting in luminescence.[183] These two works showed that laser processing could perform two tasks simultaneously – synthesize and pattern MOFs.

However, the fundamental processes and applications are not limited to those. Recent research demonstrated that laser patterning can be employed for the synthesis of metal nanoparticles, including Fe, Co, Ni, Zn, Cd, In, Pb, and Bi, using the corresponding MOF precursors (MIL-100, ZIF-12, Ni-BTC-bipy, HKUST-1, Zn-MOF-74, Cd-MOF-74, CPM-5, Pb-TCPP, and CAU-7). This innovative approach was assigned as "nanoscale laser metallurgy and patterning" (nano-LaMP) (**Figure 8**). The processing scheme involves placing MOF between two pieces of glass and irradiating it from the top. So, this way it is not only patterning, but also laser-induced transfer. By utilizing nano-LaMP, the high absorption of MOF results in photothermal conversion with temperatures reaching up to 2500 K in a reducing atmosphere. This heat affects the metal ions in the MOF, and is transferred to carbonaceous organic linkers. This leads to the formation of reductive species, which reduce metal ions to atoms, which results in the formation of metal nanoparticles. This technique not only proves to be fast and efficient for synthesizing various metals but also results in uniform particle size and, more importantly, enhanced chemical stability. For instance, the achieved Cu nanoparticles are homogeneously coated with protective graphene layers, effectively shielding them from oxidation and preserving their metallic properties for up to six months in air and humidity. Overall, nano-LaMP offers a promising avenue for advanced materials synthesis and device fabrication, presenting an exciting prospect for various applications in the future.[38] Nano-LaMP was further extended to fabricate metal alloy nanoparticle patterns using three different MOF precursors. This method allows to make highly uniform patterning with desired shapes. Depending on the method adaptation, it is possible to control the optical, electrical, and catalytic properties of Cu-Zn alloys. Even though the potential implementation is not limited to these particular metals.[184]

Whereas nano-LaMP typically completely destroys the framework and reduces MOFs to nanoparticles, laser photolysis can selectively remove photosensitive linkers without compromising the integrity of the framework, resulting in MOFs with hierarchical porosity. Wang et al.[185] followed this approach, using a 405 nm laser as the energy source for the photolysis. Since that wavelength could be absorbed by the organic ligands, it resulted in the generation of highly reactive species that formed the desired MOF structure. The use of a laser to induce photochemical reactions in this way allowed for the rapid and precise synthesis of MOFs with tailored morphologies and properties, opening the door to MOF lithography. This work, unlike others, shows the way to directly process MOF powders.[185]

4.2.3. Laser Scribing of Perovskites

Laser scribing is particularly useful for large-area displays that utilize halide perovskites. Even though the researchers should carefully consider the irradiation conditions. Perovskites are sensitive to high temperatures, so focused or high-power laser treatment may result in undesired degradation of their properties. Nevertheless, recent studies have shown that successfully optimizing laser parameters for patterning perovskites minimizes these issues. For instance, Huang et al. presented a breakthrough reversible 3D laser printing of PQDs in a transparent glass medium. Femtosecond laser induces nonlinear multiphoton absorption in the perovskite precursor solution, resulting in a 3D $CsPbBr_3$ QD structure inside the transparent glass. This method allows for the precise engineering of PQDs with high photoluminescence (PL) intensity. The reversibility in this work means that the PQD structure could be erased and rewritten using the same laser by varying the power density and exposure time. While erasing PQDs back to CsBr and $PbBr_2$ with a decrease of PL intensity caused by laser-induced defects, further laser processing reforms $CsPbBr_3$ QDs and increases the intensity back.[186] In this study, the researchers did not focus on modifying the bandgap during irradiation. Nevertheless, it is theoretically feasible to achieve such modifications. Bandgap engineering was shown using a pulsed Nd:YAG with various wavelengths (1064, 532, and 355 nm). Laser scribing facilitates the release of halide ions from the solvent, allowing for controlled ion exchange and precise tuning of the bandgap in a patterned area. Such processed perovskites were implemented for narrow blue and green photodetector arrays with a high resolution of ≈53 pixels per inch.[187] Both of these developments hold significant potential for advancing optoelectronic devices with tailored properties and functionalities.

While laser processing has shown promise in improving the performance of the devices, it can also be used to achieve precise control over the structure and properties of perovskite materials. Understanding the laser-induced processes in organic-inorganic materials is not intuitive since the mechanisms were mostly proposed for organic or inorganic ones. Kanaujia and Vijaya in turn focused on investigating the chemical/physical laser effect in organic-inorganic perovskite $(C_6H_9C_2H_4NH_3)_2PbI_4$; CHPI. Laser processing of layered perovskite films resulted in simultaneous ablation, melting and agglomeration, chemical modification and/or surface roughness, and nano/microstructuring, while not affecting the underlying glass substrate. The authors propose the dominant mechanism of single-photon absorption and highlight several details, namely, the energy diffuses out of the laser focus spot, forming a temperature-affected zone. While melting, a plasma plume containing evaporated nanoparticles appears. Finally, hot particles release heat and condense on the edges of the patterned area (**Figure 9**). This work would also be suitable for the subsection "Laser ablation of perovskites", but we keep it here to highlight the purpose of making precise patterning. The size of the processed area is controlled, as in many other works, by changing the speed, laser power, and spot size.[188]

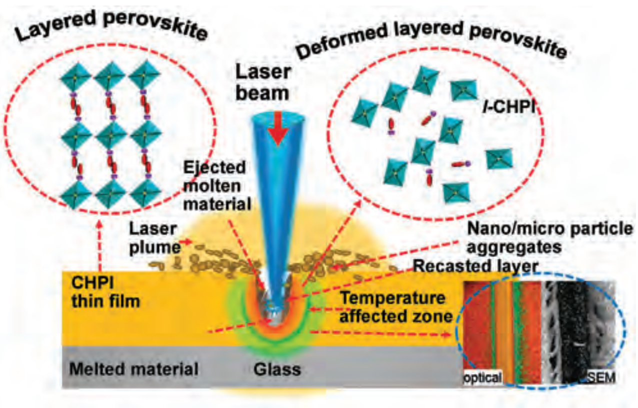

Figure 9. Laser scribing of perovskites. Used with permission.[188] Copyright 2016, Royal Society of Chemistry; permission conveyed through Copyright Clearance Center, Inc.

4.3. Laser Ablation

High-energy laser radiation is capable of inducing phase changes in material leading to its removal from the substrate. This process is called ablation. While a laser interacts with the sample, a part of the material leaves the surface in the form of electrons, ions, atoms, particles, and clusters. Each of these processes is separated in time and space.[226] Depending on the wavelength, the ablation process is usually a combination of thermal and non-thermal mechanisms. A non-thermal mechanism occurs when the photon energy is higher than the binding energy of atoms in the material, or the field created by laser radiation is high enough to break the atomic lattice and eject the ions and atoms without heating. That is why the typical choice is the femtosecond lasers.[227] Non-thermal laser ablation is often used to ablate heat-sensitive materials, such as biological tissues and polymers, as it causes minimal damage to the surrounding material.[228] On the contrary, during the thermal process, electrons absorb the energy of laser photons and transfer this energy to the atomic lattice, leading to the bond breaking and generation of high-temperature plasma.[229] The intense heat and pressure generated by the plasma expansion rapidly evaporate or sublimate a portion of the material, which is then ejected from the surface.[230–232] The material below the surface is not significantly heated, and the ablation process does not cut through the material. This approach is suitable for materials with high melting points. Briefly, laser ablation can be described in three processes: plasma formation, plasma expansion, and particle ejection. The first process strongly depends on the choice of the laser and could be thermal (ns pulses), thermal + non-thermal (ps), or non-thermal Coulomb explosion (fs). Plasma expansion depends on the energy and gas environment. Thus, choosing the pulse duration and conditions affects the ablation results the most.

Laser ablation proves to be a valuable tool due to its selective removal. This ability also allows for in situ deposition and the creation of highly precise patterns and structures at sub-micron levels, making it ideal for creating heterojunctions and other complex structures. Laser ablation has been successfully applied to modify the properties, perform structuring, and achieve specific performance of emerging nanomaterials discussed in this review.

4.3.1. Laser Ablation of MXenes

Laser ablation is currently extensively used to fabricate MXene-based electrodes. Femtosecond lasers are the most preferred choice for these purposes because of their ability to create ultra-

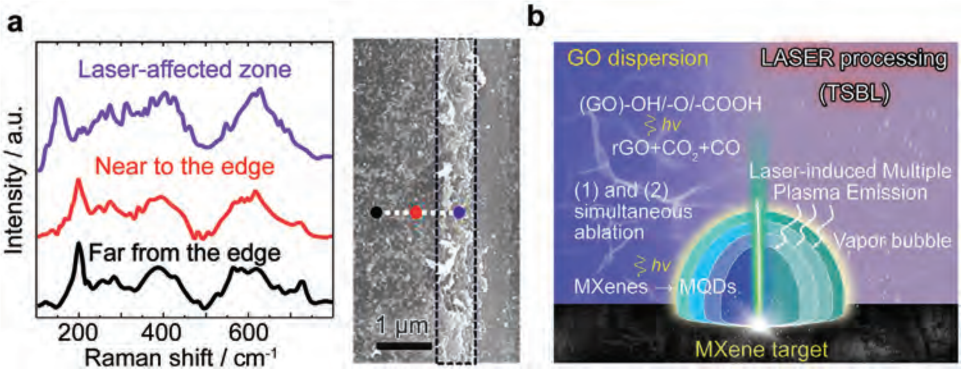

Figure 10. Laser ablation of MXenes a) Ablation to induce transformation from Ti_3C_2 to anatase TiO_2. Reproduced with permission.[189] Copyright 2020, John Wiley and Sons. b) Scheme of the novel and efficient way to synthesize MXene quantum dots/graphene composite. Redrawn with permission.[24] Copyright 2022, John Wiley and Sons.

narrow interspace widths between the electrodes. This feature is particularly advantageous for MSCs. A recent study demonstrated that the width of these lines can be finely adjusted by controlling the laser power, achieving a remarkable lateral distance of 800 nm.[189] In this work, the ablation process led to a phase transformation from Ti_3C_2 to anatase TiO_2 due to the localized heat and pressure breaking chemical bonds. This technique facilitates the high-precision alignment of the MSCs, further enhancing their performance (**Figure** 10a). Similarly, the formation of TiO_2 as an outcome of femtosecond laser ablation was previously demonstrated in another work, where microchannels were formed on the surface of MXenes. This process induced the generation of ions due to exceeding the optical breakdown threshold, molecule ionization, and dissociation. The ablation process played a key role in creating nucleation-preferable microchannels on the surface of the MXene electrode, which enabled uniform lithium deposition and improved the stability of the lithium-metal battery.[190]

To prevent the issue of stacking, MXenes were combined with other materials like MoS_2. Thus, Chen et al.[191] demonstrated the direct laser etching of a free-standing MXene-MoS_2. This technique eliminated the need for additional substrates and resulted in MSCs with a high energy density of 15.5 mWh cm^{-3} and excellent capacitance retention, maintaining 98% of its initial capacitance even after 6000 bending cycles. Combining MXenes with 1T-MoS_2 was also great for the precise temporally and spatially shaped laser ablation to reach miniaturized MSCs with the line width from micron down to record 200 nm resolution.

Laser synthesis of MXenes is another development strategy that allows the production of highly conductive surfaces with excellent energy storage and harvesting capabilities. One notable example of this approach is the study by Zang et al., which demonstrates the potential of laser processing for the fabrication of MXene-based MSCs. The researchers used a metallo-hydrogel deposited onto a substrate to synthesize transition metal carbides (TMC), including MoC_x, WC_x, and CoC_x, with a macroporous structure. The TMCs were further patterned using a laser cutter with a resolution of 25 μm to integrate electrodes for energy storage using interdigitated supercapacitors. The processing with CO_2 laser vaporized the residual solvent and carbon source. The precise control over laser parameters enables the sculpting of carbide layers, resulting in ultrathin MXene films with large surface area and relatively high electrical conductivity (≈300 S cm^{-1}). The fabricated MXene-based micro-supercapacitors (MSCs) demonstrated high capacitance, high energy density, and excellent cycling stability, demonstrating the potential of laser-synthesized MXenes for energy storage applications. Furthermore, TMCs have the potential for diverse applications, including solar-steam-generating membranes for use in harsh environments.[192]

As mentioned above, MXenes are often combined with graphene materials. A recent innovation in this context is the synthesis of MXene quantum dots/graphene composite (MQD/LRGO) through ultrafast laser processing using a temporally and spatially shaped (Bessel) laser. The method involves irradiating a $Ti_3C_2T_x$ target in GO dispersion (Figure 10b). This elegant approach promotes the simultaneous reduction of GO nanosheets and the formation of MQDs, while various laser field distribution affects the degree of reduction and uniformity. Surprisingly, except for the excellent electrochemical performance and improved mechanical strength, resulting MQD/LRGO exhibits high transparency, making it an attractive material for use in transparent supercapacitors. The electrochemical performance was evaluated using cyclic voltammetry (CV) and galvanostatic charge-discharge tests, which showed a high specific capacitance of 10.42 mF cm^{-2} (91% transmittance). This is attributed to the unique structure of the composite, providing a large surface area (up to 256.88 m^2 g^{-1}) and excellent electrical conductivity, enabling fast charge transfer and high capacitance.[24]

4.3.2. Laser Ablation of MOFs

The precise structuring of MOFs is important for practical implementations in energy, biomedicine, and electronics, and lasing is the tool to contribute to these tasks. For instance, highly efficient ZIF-8 patterning was achieved through maskless laser processing of thin ZnO layers on the top of paper-like ceramic sheets. Patterning with a tunable resolution was achieved by laser removal of nanoparticle regions with different scanning speeds. The laser-processed precursors further turned to MOF through the gas-phase reactions with ligands. Interestingly, the widening of the edges caused by ablation likely occurred due to ad-

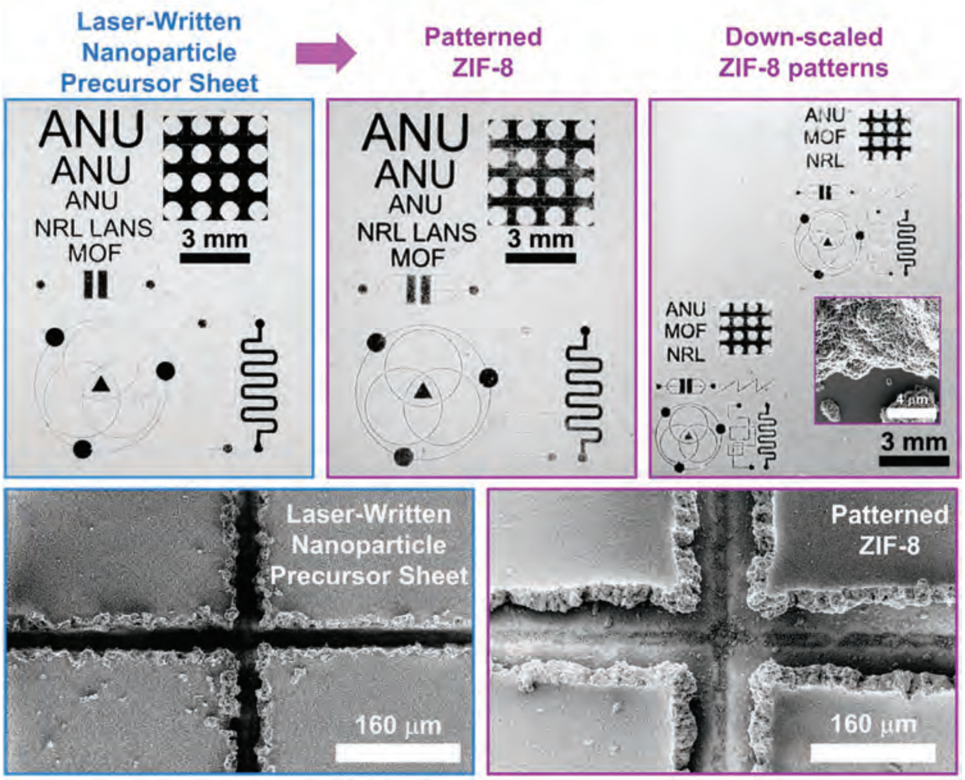

Figure 11. Laser ablation to pattern MOFs. Reproduced with permission.[193] Copyright 2021, John Wiley and Sons.

ditional local sintering of new ZnO NPs during the laser treatment (**Figure 11**).[193] The other substrates, apart from ceramics, are also useful for ablation. A recent study by Navarro et al.[194] demonstrated the potential of laser perforation of brass sheets to activate the support for further ZIF-8 uniform crystal growth on one side. Such configuration allowed for the fabrication of gas separation micromembranes aiming for future applications in carbon capture and hydrogen purification, among other areas.

Finally, laser ablation synthesis in solution was used for in situ fabrication of ZIF-67 with tailored size and geometry. It is based on the laser ablation of a Co target in a 2-methylimidazole solution. The 1064 nm pulsed Nd-YAG laser energy was absorbed by the target and converted to heat, causing the target to ablate and eject Co atoms and ions into the solution to react with 2-methylimidazole and form ZIF-67 crystals. The laser parameters, such as power, scanning speed, and precursor concentration, can be controlled to tune the size and geometry of the crystals. Laser ablation generates a plasma plume with extreme conditions (10000 K and 100 MPa) that accelerates the nucleation and growth of ZIF-67 crystals with high crystallinity, uniform size distribution, and sufficient structural stability.[195] The same strategy was applied for the fabrication of $Cu_3(BTC)_2(H_2O)_3$ MOF[196] and bismuth-based MOF.[197]

4.3.3. Laser Ablation of Perovskites

Laser ablation of perovskites is an important fundamental task since its mechanism is different compared to the processing of other photovoltaic materials. Also, precise patterning, often in an inert atmosphere to exclude exposure to oxygen and humidity, is important to produce high-quality solar cells. As a result, research efforts are more concentrated on elucidating the underlying mechanisms and exploring physicochemical processes rather than on simplified patterning applications. There are multiple attempts to reach “clean” layer interconnections without the removal of the substrate or degrading the electrical properties.[233]

To deeply understand the ablation mechanism, several research groups performed perovskites laser ablation using pulses of different durations. Among others, Turan et al. have performed a systematic investigation of perovskite ablation by using a nanosecond pulsed laser to selectively remove the perovskite absorber layer from a glass substrate, leaving behind a precisely patterned structure. The researchers utilized three laser sources operating at different wavelengths (355, 532, and 1064 nm), each with a pulse duration ranging from 7 to 15 ns and a power output varying from 10 mW to 1 W. By controlling the laser fluence and number of laser pulses, the authors were able to optimize the precise patterning process with minimal damage. The patterned perovskite solar cells exhibited high PCE and stability over time. The solar module efficiency plot showed that sheet resistance of $6\ \Omega\ \text{sq}^{-1}$ and specific contact resistance of $10\ \Omega$ mm could yield an efficiency of 18.44%. This simple yet efficient approach has great potential for meticulous patterning and large-scale solar energy harvesting.[198]Schultz et al.[199] termed the mechanism behind “classical” laser ablation, meaning that heating, melting, and evaporation have leading roles in the process, with minimal mechanical impact. The study also revealed that shifting from ns

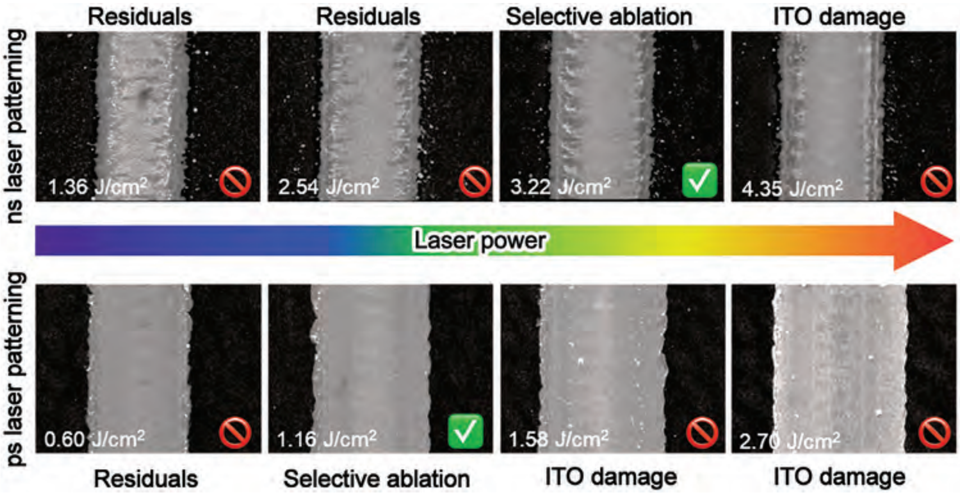

Figure 12. Laser ablation with ns and ps pulses to pattern solar cells. Adapted with permission.[199] Copyright 2020, Elsevier.

to ps pulses changes the ablation mechanism to selective removal of the metal-halide perovskite absorber layer in solar cells. Using ns pulses caused explosive boiling due to rapid heating, damaging the underlying ITO substrate, whereas the latter involved mechanically stress-assisted lift-off ablation, which affected only the perovskite layer and caused less thermal damage. Picosecond laser ablation allowed successful patterning of the solar cells without damaging the ITO layer beneath and achieving series resistance as low as ≈0.010 Ω cm^2 (**Figure 12**).[199]

Typically, ultrashort pulses are preferable to use as their time is shorter than the electron cooling time so that electrons do not transfer their energy to the lattice, which results in rapid evaporation and more efficient ablation to make “clean” patterns. During the femtosecond laser ablation, the proposed steps include the following: absorption through a two-photon process, ablation with the change of the morphology, melting and recrystallization followed by agglomeration (on the edges), and chemical and physical modifications caused by laser-induced heat and pressure. Following the Gaussian distribution, the transformation in $MAPbBr_3$ after the lasing was divided into 4 zones.[234]

Considering the versatility of laser ablation ways to process perovskites, it was investigated how different parameters (pulse duration, wavelength, fluence, and irradiance direction) affect the ablation mechanism. Three distinct mechanisms were proposed for this case: thermal ablation, thin film delamination lift-off process (before was mentioned as mechanical stress-assisted lift-off ablation), and grain lift-off process. The first process, denoted as thermal ablation, occurs for lasers with a wavelength in the region where perovskites provide sufficient absorption to reach high temperatures and induce material evaporation. Interestingly, unlike the previous works, the research by Bayer et al.[200] suggested that the main factors that determine the ablation mechanism are wavelength and irradiation direction (direct or through the substrate) rather than the pulse duration. Therefore, for the longer wavelengths where perovskites exhibit low absorption (above 800 nm for $MAPbI_3$), ablation goes through a lift-off process. This difference occurs directly from the localization of heating spots. Once the perovskites have strong absorption, laser energy converts into heat inside the perovskite layer. It induces its evaporation, but if the absorption is low, the heating is localized at the perovskites/substrate interface so that the generation and expansion of vapors in the interface create enough pressure to delaminate the film. These two mechanisms could be combined by the bottom-top irradiation (irradiation through the substrate) with the wavelength in the range of thermal ablation. The combination of the two mechanisms appears to be preferential for the perovskite patterning, minimizing cracks at the edges caused by melting. The grain lift-off ablation was observed for a 1064 nm laser (10 ps) and occurs outside the melting zone. The mechanism behind such a process is the laser-induced heating of the material in the spot center and lifting out the grain at the spot edge.[200]

4.4. Laser Cutting

Laser cutting is a form of laser ablation, based on a laser beam that cuts materials in straight lines or curves. There are different mechanisms to do that, e.g., vaporization, melting and blowing, burning in reactive gas, thermal stress cracking, and cold cutting.[235,236] The five laser-cutting mechanisms differ in how the heat from the laser beam interacts with the material.

To facilitate comparison, we introduce the scale from 1 to 100, reflecting relative energy, where 100 represents the highest applied energy (**Figure 13**). Vaporization is a high-energy process, as the laser beam heats the material above its boiling point, causing it to vaporize and eject from the surface. It requires a very high relative energy of 40 on this scale. In the case of melting and blowing, the laser beam melts the material with ≈2 times less relative energy than vaporization. The resulting molten material is then blown out, resulting in a clean cut. Burning in reactive gas is a high-energy process that heats the material to its kindling temperature, causing it to burn in a jet of reactive gas. This process requires ≈4 times less relative energy than melting and blowing. Thermal stress cracking is a low-energy process that uses a laser beam to create a thermal field in a brittle material, such as glass. This thermal field causes the material to crack along a predetermined path. In comparison with the previous cutting technique,

Figure 13. Progressive effects of increasing laser energy on a material's surface. At low energy, thermal stress and cracking occur, reaching burning in reactive gas, melting, and vaporization as energy levels rise. At the highest energy, "cold cutting" with a femtosecond laser is achieved, resulting in a precise and clean cut through the material.

this one requires 5 times less relative energy. Cold cutting is a low-energy process that uses femtosecond lasers to cut materials without generating any significant heat, producing clean cuts with minimal surface damage. In relation to the cutting mechanisms mentioned, this is the one with the highest relative energy level, ≈100.[235,236]

Femtosecond lasers were used to produce flexible and porous MXenes ribbons with uniform dimensions and significantly enlarged surface area.[201] Benefiting from these properties, the ribbons were used for the fabrication of supercapacitors with a specific capacitance of 1.3 F cm^{-2}. Ultrashort pulses are conventionally utilized for ablation and cutting, respectively, while the other important factor is the choice of wavelength. UV lasers are preferable for precise device fabrication due to their smaller spot size, while IR CO_2 lasers with a larger spot size and higher power density may induce unwanted photothermal effects on the surface and result in undesirable products.[237,238] Another work dedicated to MSCs fabrication uses a UV laser to cut blade-coated MXene films on Ni foils to create interdigitated finger electrodes with good specific capacity and excellent stability when bent up to 120°.[202]

4.5. Other Laser-Based Approaches

In addition to the well-established laser processing techniques discussed above, some less conventional methods contribute to the formation of composites and improve material properties.

For instance, a laser powder bed fusion was used to fabricate an MXene-decorated Ti alloy. In this process, the laser melts the metal powder and binds it with the MXene particles, resulting in a robust composite. Given that MXenes tend to oxidize, the process was performed in a nitrogen-rich environment. These MXene-reinforced metal matrix composites are proposed for use in aerospace, automotive, and biomedical engineering.[203]

Other extraordinary approaches are focused on the processing of MOFs. One such method is laser shock evaporation, a form of laser-induced forward transfer (LIFT) that facilitates the deposition of thin films of material onto a substrate via pulsed laser.[239] Recently, An et al.[204] utilized laser shock evaporation to synthesize a MOF nanocomposite. The process involved the synthesis of MOF and liquid metal (LM) particles, mixing them, and subjecting the mixture to pulsed laser treatment. There is a challenge with using LM as a thermal agent – they have a high surface tension, which makes it difficult to uniformly cover the surface of other materials. To overcome this issue, a laser was used as a processing tool to redistribute the LM on the complex surfaces of the MOF crystals. Specifically, a Nd:YAG laser with 1064 nm wavelength and 7 ns pulse duration was used to initiate transient heating and evaporation of the LM in a confined space. This resulted in the formation of a thin layer of LM nanoparticles (LMNPs) on the surface of the MOF crystals. The resulting MOF@LMNP composite has both the high porosity of MOF crystals and the high thermal conductivity of LM, making it an attractive material for thermal management applications.[204] The femtosecond laser treatment of MOFs also addressed the problem of producing stable and efficient ultrafine noble metal catalysts mediated with MOF-derived highly defective metal oxides. The laser was used to irradiate the Ce-MOF, which resulted in the formation of high-density defective metal oxides containing numerous oxygen vacancies. These vacancies provide active sites for the deposition of ultrafine noble metal nanoparticles for highly efficient and stable catalysts due to the strong interaction between the metal nanoparticles and the defective metal oxides. In particular, that was done to make a laser-induced CeO_2-mediated Pt catalyst (L-Pt@CeO_2). A Ce-based MOF was used as the starting material and was irradiated with a laser in the presence of a Pt precursor. The laser-induced reduction of the precursor materials generated the active catalyst and CeO_2 support material. This laser processing technique demonstrated high efficiency, with a conversion rate of over 90% of metal ions to metal nanoparticles. Moreover, the laser-reduced metal nanoparticles exhibited stability and resistance to agglomeration, which is desirable for their use as catalysts.[205] The recent work of Van Lam et al. on the laser-induced sulfurization of nickel-based MOFs serves as an example of one more method for improving the stability and performance of MOFs. By impregnating the MOF with sulfur and using a pulsed CO_2 laser, the authors were able to produce ultrasmall and uniform metal sulfide nanoparticles (NiSx, CoSx, and MnS/MnO) in just a few minutes. The laser process involved carbonizing the organic ligands in the MOF into porous carbon, which reduced the metal ions in the MOF to metallic nanoparticles and triggered the graphitization of the carbon, producing metallic nanoparticles confined in graphitic carbon. The laser-sulfurized MOFs exhibited outstanding electrochemical performance and cycling stability, indicating potential for future energy material design.[206] Another technique for depositing thin films on a substrate via pulsed laser is femtosecond pulsed-laser deposition (femto-PLD). While it may not be straightforward to deposit pristine ZIF-8, it can be improved by using hybrid ZIF-8 films with polyethylene glycol 400. PEG serves as a carrier for ZIF-8, aiding in its ablation under ultrahigh vacuum conditions.The femto-PLD was performed using a laser with a wavelength of 516 nm and pulse width of 442 fs to ablate the hybrid ZIF-8/PEG. Thus, starting from PEG-modified ZIF-8 powder, pure ZIF-8 films were obtained on sapphire substrates.[207]

4.6. Summary of the Laser Impact on Emerging Nanomaterials

Section 4 brings together the most notable papers in the research and engineering direction of laser processing of MXenes, MOFs, and perovskites published up to date. The most valuable methods for processing these materials are laser scribing and laser ablation. Laser scribing is useful for all three materials and is especially used in practice for the fabrication of the supercapacitor electrodes. Localized laser treatment demonstrates its ability to enhance crystallinity, electrical properties, promote carbonization, and, in the case of MOFs, fine-tune pore sizes. Furthermore, laser patterning was used to synthesize metal nanoparticles using MOF precursors. Laser ablation turned out to be a particularly useful tool for patterning perovskite solar cells. The manuscripts dedicated to this topic are the most fundamental among all the papers cited in this review, as a deep understanding of mechanism and parameters influence will significantly affect the performance of perovskite optoelectronics. In addition, high-powered lasers find application in the precise cutting of emerging materials to create ribbons or devices of specific shapes.

The most used lasers for all the cases are Nd:YAG, and CO_2, while the pulse duration varies from short (ns) to ultrashort (fs, ps) pulses, with very few works utilizing wider ones (ms). The short pulse lasers offer more precise size control and energy transfer due to limiting the thermal effects, as well as faster processing for the shorter pulses.[162] The “optimal” combination of the material, laser source, power, and pulse duration results in different outcomes, from local surface modification to a complete cutting.

Given the promising results achieved by now and the existing gaps in our knowledge, future developments should be focused on the following directions:

- Enhanced efforts on optoelectronics. As discussed in Section 1, the optical properties of these materials have not yet been fully discovered. Nevertheless, the materials already exhibited potential for application in solar cells, LEDs, and photodetectors.[22,240] Section 5 touches on some of these findings, including the flexible ones, but there is plenty of room for further in-depth research.
- Theoretical studies. Most of the works rely only on experimental data, while future research should also involve theoretical investigations of the effect of the laser. Simulations can provide valuable insights into the underlying processes, technology optimization, and a deeper understanding of these materials' nature.
- Fabrication of composite materials. Laser processing showed its efficiency in forming flexible composites with different nanomaterials.[19,241] This section showed several examples with all three materials. However, there are almost unlimited options for the combinations and tuning of the materials, and future research will lead to the fabrication of new, flexible, lightweight, and conductive composites.
- Technical improvements and scaling up. The engineering optimizations would result in more reproducible results, large-scale fabrication, and commercialization.

High interest in the various processing techniques indicates that this field will continue developing, resulting in new functional materials for various purposes, including optoelectronics and photocatalysis.

5. Applications of Laser-Processed Emerging Nanomaterials in Flexible Optoelectronics

In Section 4, we discussed the approaches to synthesize and pattern emerging nanomaterials through laser processing. This section provides an overview of the use of these laser-based strategies, aiming for the fabrication of flexible optoelectronic devices based on MXenes, MOFs, and perovskites. Furthermore, this section identifies opportunities for future research in this exciting field. **Table 2** summarizes the key findings from this section, providing a useful reference for the readers, showing that the use of laser-processed emerging materials has the unlocked potential in flexible optoelectronics.

5.1. Laser Processing for MXenes Optoelectronics

As was mentioned above, laser processing of MXenes is extensively used for MSCs and electronics. At the same time, the applications in optoelectronics are still limited, with only a few recent studies demonstrating the material's potential (**Figure 14**a). Such a low interest could be explained by the bandgap values not entirely matching the demands for LEDs or photodetectors, potentially unwanted surface reactivity, and the currently insufficient level of technology optimization. Despite that, recent progress shows the potential to overcome these challenges by combining MXenes with other materials, making QDs, or discovering and exploiting new properties. Photolithography is a common technique used in the semiconductor industry to pattern materials onto a substrate.[252] By using this approach, MXene films have been patterned into a pixel array on a SiO_2/Si wafer, with a resolution of up to 2 µm, which is a significant improvement over other large-area patterning methods that typically have resolutions of 10 µm or more (Figure 14b). The process involves spin-coating a photoresist layer onto the MXene film, exposing the film to UV light through a mask over certain areas, and dry-etching the MXene film. This multistep processing resulted in a high-performance photodetector with a light-to-dark current ratio of $6.22 \cdot 10^6$ and specific detectivity of $7.73 \cdot 10^{14}$ Jones.[242] Similarly, Kim et al.[253] proposed using a photomask to expose a pattern of interdigitated electrodes on a rigid Si/SiO_2 substrate. Next, an MXene composite was spin-coated onto the patterned substrate. After the film dried, the photoresist was removed with acetone, and a polyimide layer was deposited on the MXene layer. Finally, the SiO_2 layer was etched away with a strong acid, leaving the MXene electrodes on the PI film. This process yields MXenes on a flexible substrate via photolithography and transfer. The need for compatible photoresist and etching processes limits photolithographic patterning of MXene films on flexible substrates. This

Table 2. The use of laser-processed emerging materials in flexible optoelectronics.

Laser strategy	Performance	Application	Reference
MXenes			
Laser photolithography	light-to-dark current ratio of $6.22\cdot10^6$; D* of $7.73\cdot10^{14}$ Jones	photodetectors	Li et al., 2022[242]
Laser ablation and patterning	under 808 nm: R of 11.59 AW^{-1} and D* of 4.41×10^{11} Jones; under 532 nm: R of 84.77 AW^{-1} and D* of 3.22×10^{12} Jones; image sensor arrays (25 × 50 pixels)	photodetectors	Ren et al., 2020[22]
Laser synthesis – nano-MXenes terminated with halogens via the pulsed laser irradiation	enable interfacial ionic stabilization resulting in PCE up to 24.17%	PSCs with MXene interfacial layer	Guo et al., 2022[243]
MOFs			
Laser scribing – synthesis	high broadband light absorption; P_v of 42 000 kW m^{-3}	solar steam generator	Jiang et al., 2020[244]
Laser ablation in liquid – synthesis	precise morphological and structural control	potentially applied in various optoelectronics fields	Ribeiro et al., 2019[195]
Laser ablation in liquid – synthesis	intense red emission at 614 nm under UV excitation with $\Phi = 40\%$	potentially applied in various optoelectronics fields	da Costa and de Azevedo 2016[245]
Perovskites			
Laser annealing – surface treatment	PCE of 20.23%	PSCs	You et al., 2020[168]
Laser-induced heat treatment – surface treatment	PCE of 13.03%	PSCs	Trinh et al., 2020[246]
Laser annealing – surface treatment	PCE of 12%	PSCs	Jeon et al., 2016[247,248]
Laser ablation	PCE of 15% over 83 cm^2 active area	PSCs	Palma et al., 2017[249]; Razza et al. 2021[250]
Laser patterning – microstructuring	precise patterning; efficient photoluminescence at ≈518 nm	LEDs	Kanaujia and Vijaya, 2016[188]
Laser ablation – patterning	high-precision and high-quality structures; luminance of 18.390 cd m^{-2}; current efficiency 1.9 cd A^{-1}	LEDs	Liang et al., 2022[248]
Laser photolithography ablation – patterning	highly ordered nanoholes and nanostripes (250 nm), metasurfaces (500 nm), nanowire lasers (500 nm)	various optoelectronic devices	Zhizhchenko et al., 2020[251]

Note: D*, specific detectivity; Φ, quantum yield; PCE, power conversion efficiency; PSCs, perovskite solar cells; P_v,volumetric thermal power; R, photoresponsivity.

limitation has hindered the widespread adoption of photolithography for this application.

Direct laser patterning has been developed as a more versatile and compatible approach to patterning MXene films on flexible substrates. This route was used to fabricate image sensor arrays from MXene-perovskite hybrid materials. In this process, a femtosecond Nd:YAG laser is used to selectively remove the MXene layer on the perovskite surface in three stages to form patterned structures with high precision and resolution. The first step represents laser processing to pattern the MXene film on the glass substrate, using a ns laser to obtain multiple channels. The perovskite layer is further deposited on the top of this surface. In the second stage, the as-deposited perovskite/MXene/glass is transferred into ambient air again, and a second laser scribing process with a lower power output (0.25 W) is used to remove the excess photoactive layer. In the last stage, a third laser scribing process with laser power of 2 W is used to split the perovskite photoactive layers and the MXene electrodes with a width of 120 µm. This step is necessary to isolate each pixel. Such patterned MXene-perovskite hybrid materials exhibit high photoresponsivity (R) and specific detectivity (D*) in the visible to NIR range (e.g., under 808 nm: R of 11.59 AW^{-1} and D* of 4.41 × 1011 Jones, and R of 84.77 AW^{-1} and D* of 3.22×10^{12} Jones under 532 nm), making them suitable for the use in photodetection and image sensor arrays (25 × 50 pixels) with high resolution and sensitivity (Figure 14c).[22] MXenes are promising for interfacial engineering in perovskite solar cells due to their layered structure. A laser-based technique produced nano-MXenes with tailored halogen terminations, stabilizing the interface between the electron transport layer and the perovskite layer. Nano-MXenes formed strong ionic bonds with the perovskite, which retarded the lattice instability that can degrade PSCs (Figure 14d). Consequently, PSCs with nano-MXenes showed excellent long-term stability, retaining 85% of their initial PCE after 1000 h under thermal stress

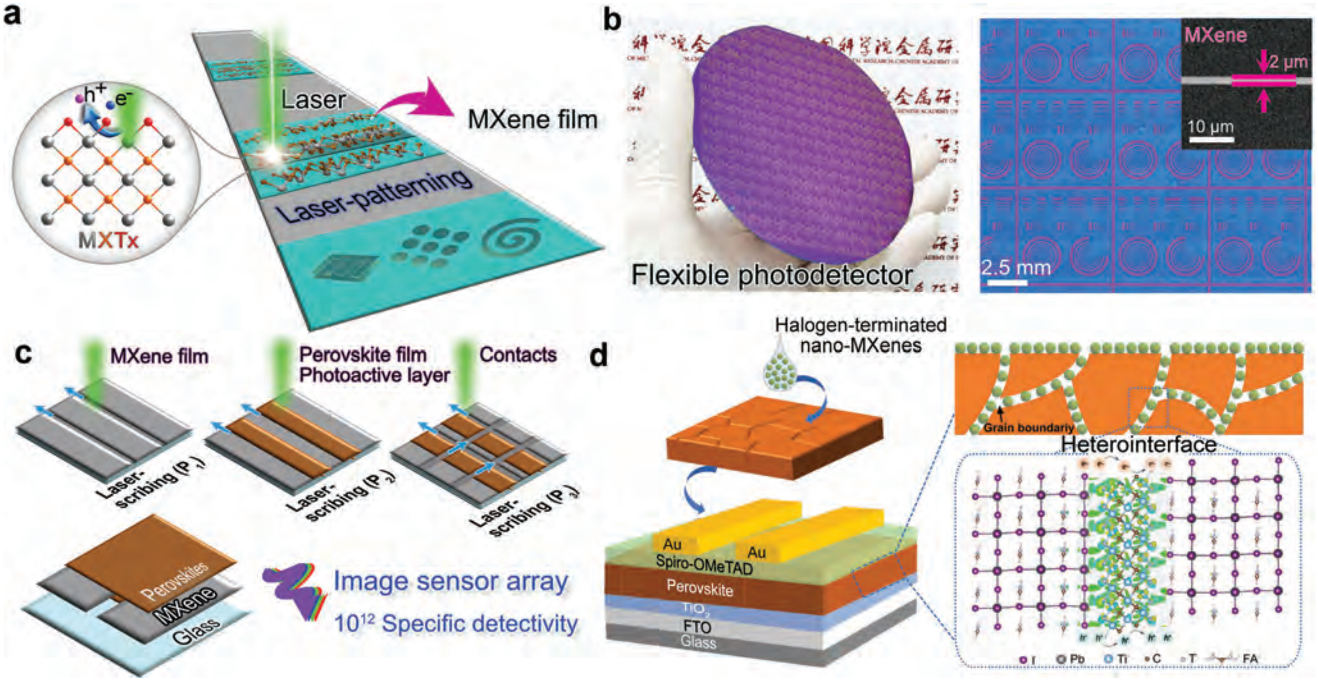

Figure 14. a) Schematic illustration of MXene laser patterning. b) Laser patterning of a MXene/Si combination; photodetector and optical images of the patterns with microscale resolutions. Reproduced with permission.[242] Copyright 2022, John Wiley and Sons. c) Scheme of the laser-scribing process to fabricate a large image sensor array for vis-NIR photodetection. First, laser scribing (P_1) is used to pattern MXene film, and then (P_2) is used to remove the excess of the photoactive layer. The third laser-scribing (P_3) splits the perovskite and MXene layer in perpendicular directions. Redrawn with permission.[22] Copyright 2020, Royal Society of Chemistry. d) Halogen-terminated nano-MXenes and perovskites by laser processing for highly stable hybrid perovskite. Reproduced with permission.[243] Copyright 2022, John Wiley and Sons.

of 85 °C and 1000 h under maximum power point operation conditions, paving the way for their commercialization.[243] Additionally, laser scribing could be used to create both patterns and functional nanostructures on MXene surfaces, such as nanoripples that are aligned with the laser polarization. This process is reversible, and the material can be switched back and forth between a flat and rippled morphology by further laser illumination. Reversible nanorippling could be used to tailor the functionality of MXenes to control light absorption and reflection. This is because the nanoripples can trap and scatter light, which is useful to enhance the performance of MXene-based devices in optoelectronics applications.[254]

5.2. Laser Processing for MOFs Optoelectronics

There are not numerous but several recent emerging examples of the use of MOFs for flexible optoelectronics. The graphene-metal composite synthesized through lasing by Jiang et al.[244] is one such example. The laser irradiation induced two processes, the first of which is photothermal transduction of laser energy by Cu^{2+} ions in MOF, resulting in the rise of local temperature up to 2200 K. Such high temperatures simultaneously initiate the second process – pyrolysis of organic species in MOF. Pyrolysis creates a 3D graphene skeleton and makes a reducing atmosphere to reduce Cu^{2+} ions to Cu nanoparticles, which get incorporated into the graphene. In the end, the resulting material exhibited high broadband light absorption and was used to demonstrate an efficient solar steam generator with a P_v of 42 000 kW m^{-3}.[244] Laser ablation in liquid is another tool that contributes to optoelectronics by forming a highly luminescent MOF $Eu(TMA)(H_2O)_4$. The resulting MOF had a well-defined rod-like shape with a maximum length of 2 μm. The optical properties of Eu-MOF were characterized by PL spectroscopy, which showed intense red emission at 614 nm under UV excitation with a quantum yield of 40%.[245] The highly efficient luminescent MOFs are crucial for a range of applications in optoelectronics, sensing, and imaging.

5.3. Laser Processing for Perovskite Optoelectronics

The combination of high absorption coefficients, long carrier diffusion lengths, and tunable bandgap makes perovskites more obvious candidates for use in optoelectronics than MXenes and MOFs. Laser processing strategies (**Figure** 15a) proved to be useful in modifying crystal structure and surface properties, as was highlighted in the previous section. Unlike two other emerging materials whose applications are mostly focused on supercapacitors, the implementation of laser irradiation to perovskites is specifically aimed at applications such as LEDs, photodetectors, and solar cells.

Perovskites are among the materials whose laser processing stages, underlying mechanisms, and parameters were investigated in detail as these aspects are critical to reaching maximal crystallinity (Figure 15b), precise patterning (Figure 15c–e), and

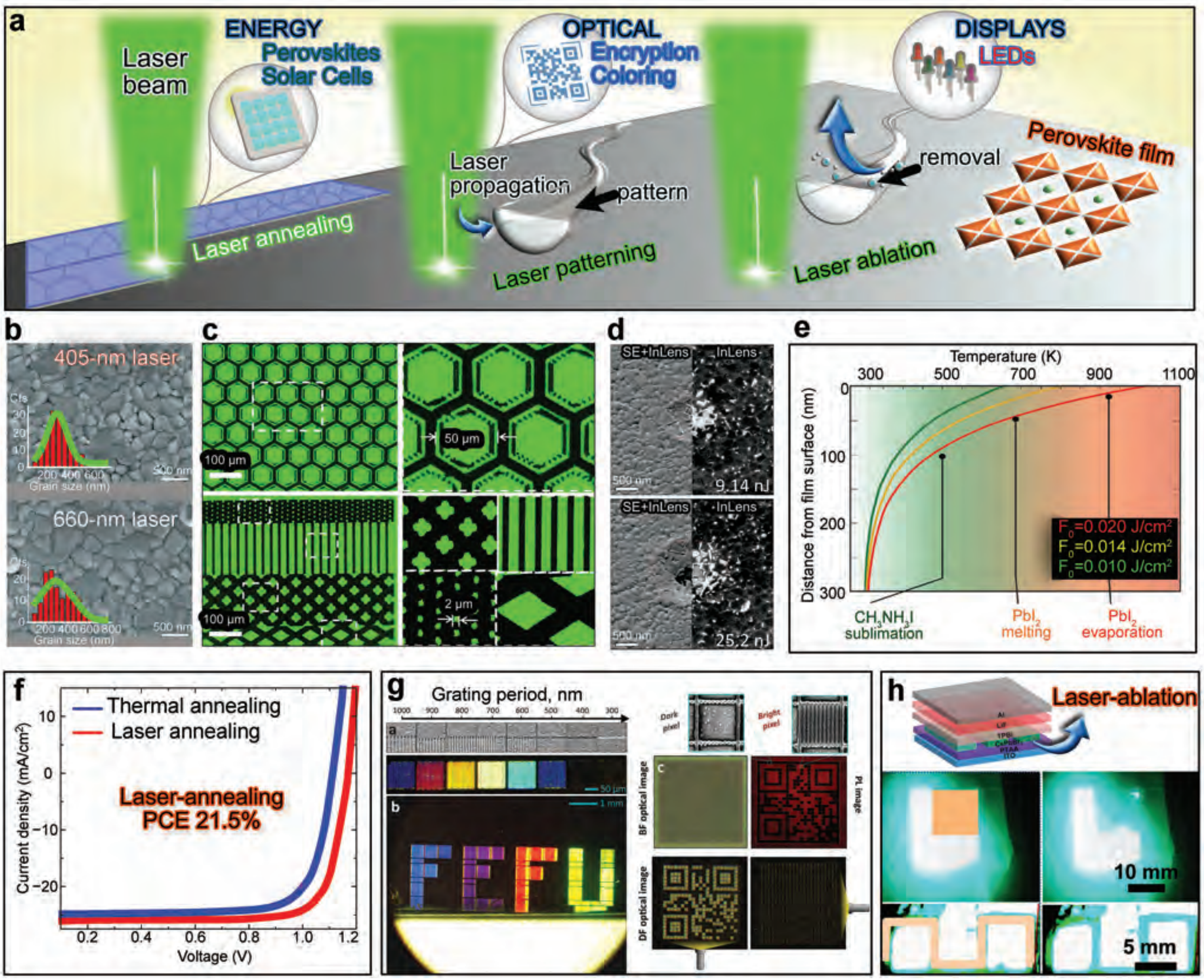

Figure 15. a) Schematic representation of the laser processing techniques for perovskite optoelectronics. b) SEM images of perovskite film by laser annealing with the size distribution. Used with permission.[168] Copyright 2020, Royal Society of Chemistry. Permission conveyed through Copyright Clearance Center, Inc. c) Fluorescence images of laser-patterned $CsPbBr_3$ film. Reprinted (adapted) with permission.[248] Copyright 2022, American Chemical Society. d) SEM images of $MAPbI_3$ film irradiated by a single fs pulse. Reproduced with permission.[251] Copyright 2020, John Wiley and Sons. e) Laser thinning mechanism of $MAPbI_3$ film. Reproduced with permission.[251] Copyright 2020, John Wiley and Sons. g) Laser patterning of $MAPbI_3$ for different optoelectronic devices. Reproduced with permission.[251] Copyright 2020, John Wiley and Sons. h) LED device structure and images created using a $CsPbBr_3$ film by laser ablation. Reprinted (adapted) with permission.[248] Copyright 2022, American Chemical Society.

enhanced device efficiency. Perovskite solar cells (PSCs) have rapidly achieved high PCEs in recent years.[255] However, PSCs are still susceptible to degradation, which can be caused by external and intrinsic factors.[256,257] Nanosecond pulsed UV laser was used to improve both the stability and efficiency of PSCs without compromising the thickness of the film. The laser-increased PCE up to 19.3% for planar PSCs with a triple cation composition, which is an improvement over the 18.0% PCE achieved without laser annealing. Additionally, some devices retain their performance for up to 1000 h. Even higher PCE was achieved in the methodological research of the influence of 405, 450, and 660 nm continuous wave lasers on crystallinity and grain size of $MAPbI_3$ and the mixtures ($(CsPbI_3)_{0.05}(FAPbI_3)_{0.95}$-$(MAPbBr_3)_{0.05}$). A PCE of 20.23% was achieved by using a 405 nm laser with a scanning speed of 25 mm min^{-1} and a laser power of 150 mW. The quality of the laser-annealed perovskite films is closely tied to the photovoltaic efficiency of the PSCs, as the crystallinity of the films is a critical factor (Figure 15f). This suggests that ultrafast laser-annealing is a promising technique for the fabrication of highly efficient PSCs.[168] Processing with a longer wavelength of 1064 nm with a pulsed (ns) laser caused an increase in the crystallinity and grain size of the perovskite films, contributing to a relatively high PCE of 13.03%.[246] The same laser crystallization of $MAPbI_3$ with a 1064 nm laser also showed an increase of PCE up to 12%, indicating that the wavelength is not as crucial a parameter as the power density, which greatly affects the grain size. The photothermal heating, which is triggered by the absorption of light by the substrate, was shown not only for rigid substrates like glass ($MAPbI_3$-PEDOT:PSS-ITO-glass), but also adapted to flexible systems (ITO-poly(ethylene-2,6-naphthalate)).[247]

Besides these findings, laser ablation was used in many other works to scale up and fabricate pixel-structured large-area perovskite solar modules.[249,250] For these purposes, three-step laser processing was coupled with interface engineering. Patterning each structural element in solar panels was used to create homogeneous, interconnected individual solar cells. First, laser ablation was used to pattern glass/transparent conductive oxide (transparent electrode) to separate individual solar cells and limit the impact of resistance increase. The second ablation step removed deposited ETL, HTL, and perovskite layers to clean transparent conductive oxide vertical interconnections. Finally, the third ablation step was used to create a pattern on the second electrode. In the end, structured solar modulus achieved a PCE of 15% over an 83 cm^2 active area.[250] This three-step patterning was also used to create a SnO_2/meso-TiO_2-based fully flexible perovskite module, which showed a PCE of 8.8% over a 12 cm^2 active area.[258]

The fabrication of highly luminescent perovskite stripes and surfaces with a size of up to 250 nm was achieved by femtosecond pulsed laser ablation.[251] Investigated $MAPbI_3$ has extremely low thermal conductivity of $\approx 10^{-3}$ W cm^{-1} K^{-1}, which results in low heat dissipation during the processing, which, in turn, preserves PL properties. This work strongly focuses on the mechanism behind it, proposing that laser ablation takes place in several stages. The first and less energetic stage is the sublimation of organic parts at locally induced temperatures $\approx$600 K with the formation of PbI_2-rich regions. The second and third stages are attributed to the changes in PbI_2 itself, namely melting at 680 K and evaporation at 920 K. This explanation is close to the one proposed by Kanaujia and Vijaya[188] discussed above in Section 4, but more precise. This work shows the implementation of pixel structures for displays, linear and non-linear optical elements, optical information encryption, and surface coloring (Figure 15g).[251]

Although ablation is the most used, it is not the only laser-based strategy to create perovskites optoelectronics. Liang et al.[248] recently showed an efficient way to achieve perovskite crystallization and patterning via laser transfer to a target substrate. They used inorganic $CsPbBr_3$, which indicated that, under the right conditions, laser processing is efficient for any type of perovskites, attributing the mechanism to nonlinear multiphoton absorption. The obtained low-defective and precisely patterned (pixel width up to 2 µm) structures showed remarkable emission (18.39 cd m^{-2} and 1.9 cd A^{-1}), being excellent choices for fabricating LEDs with improved performance (luminescence 490 cd m^{-2}, and 0.27 cd A^{-1} current efficiency) (Figure 15h).[248]

Besides patterning films, a more novel and efficient way is patterning PQDs for the fabrication of miniaturized micro-LED displays, anticounterfeiting applications, and nanolasers, even though the direct laser patterning might be challenging because of the ligand removal and losing the intrinsic high PL of PQDs. Zhan et al.[259] proposed in situ laser fabrication and gamma phase patterning of $CsPbI_3$ PQDs, in which the PL quantum yield was not affected, remaining at 92%. Such processing was implemented to fabricate a grating, showing different colors from dark blue (453 nm) to red (702 nm), varying the angle from 46° to 58°, and fluorescent patterns of arbitrary shapes visible under the UV light.[259]

6. Application of Laser-Processed Emerging Materials in Photocatalysis

Photocatalysis is an important developing research field that involves the use of materials to accelerate chemical reactions through the absorption of light. To be an efficient photocatalyst, the material should have a bandgap that allows absorption in a wide range. It is highly desired to have a high charge carrier mobility and the highest possible surface area. MXenes, MOFs, and perovskites contribute to the development of this exciting research area, while laser processing serves as an efficient tool to modify material properties to increase their performance.

Laser processing of MOFs was used to produce highly efficient 3D graphene-based catalytic membranes (3D-GCM) with active metal nanoparticles. In this work, Huang et al.[260] used MOFs as a precursor of metal ions to be incorporated in sintered reduced graphene oxide sheets by a single-step laser scribing (1064 nm, 80 ns pulse width). This facile approach makes it possible to integrate different metallic species into the graphene structure, resulting in Cu@3D-GCM, Cu/Ag@3D-GCM, and Cu/Pd@3D-GCM materials for HER. Among all others, Cu/Pd@3D-GCM showed the highest H_2 catalytic generation at a rate of 1.3474 mmol g^{-1} h^{-1}.[260] The close strategy was used to fabricate MOF-derived Co nanoparticles. They were further combined with nitrogen-doped porous graphene. Such electrodes were fabricated on a kapton substrate and used for water dissociation with OER and HER, showing an efficiency close to the commercial Pt/C.[261] Laser processing was used to produce transition-metal carbides (TMCs) from MOFs. Wu et al.[262] were able to obtain HfC, ZrC, TiC, V_8C_7, α-MoC, Cr_3C_2, and FeC_x nanoparticles with homogeneous sizes (between 6 and 20 nm). There are three criteria that should be fulfilled to achieve this: 1) sufficient temperature induced by laser heating to activate metal reduction, 2) efficient contact between metallic and organic species for homogeneous reaction, and 3) instant cooling and heating to prevent particle coalescence. Achieving these conditions was possible when using MOFs. In particular, FeC_x nanoparticles were functionalized with nitrogen groups and used as catalysts in Fischer-Tropsch synthesis. Such catalysts are one of the most efficient for CO conversion, with an efficiency of 94%.[262]

Gunina et al.[263] demonstrated the application of laser-processed HKUST-1 MOF for the decomposition of dyes. The authors investigated the impact of various laser processing parameters (pulse width, frequency, and laser fluence) on the structure, properties, and performance of several MOFs. Their findings revealed that HKUST-1 treated with an fs laser operating at 100 kHz exhibited the most noteworthy photocatalytic activity against rhodamine 800. Such a performance was attributed to the laser-induced conversion of MOF into melted particles, characterized by a combination of metal oxides and carbon species.

As for the use of MXenes, laser ablation of several different MAX phases, including Ti_3AlC_2, Ti_2AlC, Nb_2AlC, and V_2AlC, was used to produce quantum dots (MxQD). Their semiconducting nature and tunable bandgap made them highly promising in photocatalysts for HER, with a final H_2 generation rate of 48.6 $mmols_{H2}/g$ for 24 h. Even fabricated at non-optimized conditions and agglomerating, these materials are among the best photocatalysts reported.[264]

Laser-assisted chemical vapor deposition (LCVD) was used in the fabrication of nanostructured $NaTaO_3$ and $SrTiO_3$ thin films for photocatalytic hydrogen evolution. The LCVD process was conducted on a stainless steel substrate. First, the precursors for perovskite films (Na(dpm) and $Ta(O\text{-}i\text{-}C_3H_7)_5$ for $NaTaO_3$, and $Sr(dpm)_2$ and $Ti(O\text{-}i\text{-}C_3H_7)_2(dpm)_2dpm)$ were vaporized and transferred into the LCVD reactor chamber which was filled with an Ar atmosphere supplemented with O_2. The substrate was preheated to 673 K, and throughout the synthesis, it was irradiated with CW Nd:YAG laser (1064 nm) with powers ranging from 43 to 64 W. The resulting temperature upon irradiation was measured to range between 793 and 823 K, with these two temperature values proving critical as they yielded different crystalline forms of the perovskite films. Specifically, synthesis at 793 K led to orthorhombic crystals for $NaTaO_3$, while 823 K resulted in the monoclinic structure. Similarly, two distinct phases were observed for $SrTiO_3$: pure cubic $SrTiO_3$ at 793 K and cubic $SrTiO_3$ with tetragonal Sr_2TiO_4 at 823 K. Among them it was shown that orthorhombic $NaTaO_3$ exhibited a remarkable hydrogen evolution rate of 5672 μmol g^{-1} h^{-1}, and cubic $SrTiO_3$ 494 μmol g^{-1} h^{-1} upon UV light irradiation. These rates were significantly higher than the powder forms of the same compounds (430 and 4 μmol g^{-1} h^{-1}, respectively). This substantial improvement was attributed to more efficient charge separation, resulting in reduced recombination rates facilitated by the formation of roof-like and cauliflower-like morphologies of $NaTaO_3$ and $SrTiO_3$ thin films, respectively.[265]

Andrei et al.[266] investigated the efficiency of LaFeO3 grown on Nb: SrTiO3 substrate using pulsed laser deposition (PLD) for oxygen evolution reaction. The study also explored the impact of oxygen pressure during growth on the photoelectrocatalytic performance of perovskite structures. By varying the oxygen pressure, the authors achieved perovskite thin films with different morphologies. Notably, a pressure of 0.9 mbar resulted in the highest roughness of 15 nm (root-mean-square roughness), whereas all other pressures yielded roughness values below 2 nm (0.05, 0.25, 0.3, 0.6 mbar). In addition to modified roughness, the sample prepared with 0.6 mbar exhibited superior crystallinity and lower defect concentrations. This sample demonstrated the highest photocatalytic performance, producing a photocurrent of $\approx$1.6 mA cm^{-2} at the applied potential of 1 V (vs Ag/AgCl) and illumination with a 405 nm chopped laser (5 mW output power). Such a high value was attributed to the reduction of oxygen vacancies at the thin film's surface resulting in "optimal" concentration. Excess oxygen vacancies in perovskite films were noted to act as charge traps for photogenerated carriers, leading to suppressed photocatalytic activity.[266]

Interestingly, until now, laser-processed perovskites were not exploited for photocatalysis. This might be attributed to other common methods, like solution-based synthesis or template-assisted methods, which offer good surface reproducibility and stable composition with possibilities that have not yet been exhausted.[267] However, considering that perovskites themself are promising photocatalysts[268] and laser methods are getting widespread for perovskites, we anticipate future research works will cover that topic, for instance, by reducing surface defects or engineering surface energy.

7. Summary and Outlook

Flexible optoelectronics, wearables, and photocatalytic platforms are experiencing rapid growth in parallel with the continuous interest in nanomaterials. This review showed the immense potential offered by MXenes, MOFs, and perovskites in shaping the next generation of efficient devices. We provided a concise overview of these materials' properties and synthesis techniques, focusing on laser-based strategies for manipulating their structural, optical, and electronic characteristics. Despite the seemingly straightforward concept of laser treatment, the range of processing techniques is remarkably diverse, including laser scribing, laser annealing, laser ablation, cutting, transfer methods, and several not-that-well-known approaches, for instance, so-called sulfurization, or pulsed laser deposition. All these have already been applied to tailor these three emerging materials. Our work summarizes aspects from the foundational principles to real-world applications, emphasizing the effectiveness and promising prospects of lasing.

While laser ablation, cutting, transfer, and annealing have been widely investigated for years in application to these emerging materials, a few curious examples should be highlighted: laser processing applied for the synthesis of MOFs with controlled size and crystallinity or for MQDs – a material with yet unexplored potential. Implementing nano-LaMP to fabricate nanoparticles or inducing oxygen-containing defects for enhanced deposition of noble metals are also creative and even unexpected findings.

For all the materials considered in this review, stability under laser irradiation is a crucially important factor, and there are yet unexplored regimes that allow patterning with the required chemical composition or structure. However, investigating the full potential of laser processing is strongly limited by an expansive parameter space. Each of the parameters, from the choice of wavelength to spot size, scanning speed, or focusing, significantly affects the whole system, especially going down to the nanolevel. Counting that the processes are material-dependent, this might get even more challenging. The complexity of the task can be reduced by investigating both – the mechanisms of the occurring chemical reactions and other effects, including the transfer of the ablated material. Recent works on using machine learning to optimize experimental parameters will also give a significant boost to obtaining high-performance structures.[269–271]

Unavoidably, when it comes to laser processing, many reports state the result as a function of laser processing parameters rather than investigating the mechanisms behind it. To some degree, this situation reflects the complexity of investigating the laser processing fundamentals, which means that advanced measurement tools and verified models that consider multiple effects are needed.

Another significant limitation to the widespread adoption of laser processing is its lack of reproducibility. This issue poses a substantial barrier to commercialization, as different methods and slight variations in material composition can yield disparate morphologies, compositions, and properties. This variability makes it challenging to anticipate and establish standardized performance criteria for devices based on these emerging nanomaterials.

To go beyond and get to another level of using these materials and get efficient processing with lasers, there is a need for interdisciplinary collaborations between materials scientists, engineers, chemists, and physicists. There are numerous applications of emerging nanomaterials in flexible optoelectronics, and laser processing has the potential to enhance their performance significantly. The current findings represent only a fraction of the possibilities that can be unlocked through further exploration and innovation.

Acknowledgements

The work was supported by a Russian Science Foundation grant No. 23-42-00081. “Flexible and durable multi-functional sensors without cross-talk” (China-Russia Collaboration project NSFC number 62261136551)

Conflict of Interest

The authors declare no conflict of interest.

Keywords

laser processing, metal-organic frameworks (MOFs), MXenes, optoelectronics, perovskites, photocatalytic materials

Received: December 15, 2023
Revised: February 29, 2024
Published online: April 3, 2024

---

[1] J. Du, H. Yu, B. Liu, M. Hong, Q. Liao, Z. Zhang, Y. Zhang, *Small Methods* **2021**, *5*, 2000919.
[2] H. Zhu, Y. Shen, Y. Li, J. Tang, *J. Semicond.* **2018**, *39*, 011011.
[3] H. Zhang, J. A. Rogers, *Adv. Opt. Mater.* **2019**, *7*, 1800936.
[4] Q.-B. Zhu, B. Li, D.-D. Yang, C. Liu, S. Feng, M.-L. Chen, Y. Sun, Y.-N. Tian, X. Su, X.-M. Wang, S. Qiu, Q.-W. Li, X.-M. Li, H.-B. Zeng, H.-M. Cheng, D.-M. Sun, *Nat. Commun.* **2021**, *12*, 1798.
[5] K. Behrman, I. Kymissis, *Nat. Electron.* **2022**, *5*, 564.
[6] Y.-H. Won, O. Cho, T. Kim, D.-Y. Chung, T. Kim, H. Chung, H. Jang, J. Lee, D. Kim, E. Jang, *Nature* **2019**, *575*, 634.
[7] H. P. T. Nguyen, S. Arafin, J. Piao, T. V. Cuong, *J. Nanomater.* **2016**, *2016*, 2051908.
[8] A. D. Bartolomeo, *Nanomaterials* **2020**, *10*, 579.
[9] P. Kumbhakar, C. C. Gowda, C. S. Tiwary, *Front. Mater.* **2021**, *8*, 721514.
[10] X. Xie, N. Zhang, *Adv. Funct. Mater.* **2020**, *30*, 2002528.
[11] M. Treger, A. Hannebauer, A. Schaate, J. L. Budde, P. Behrens, A. M. Schneider, *Phys. Chem. Chem. Phys.* **2023**, *25*, 6333.
[12] J. A. Siddique, A. Numan, in *Contemporary Nanomaterials in Material Engineering Applications*" (Eds: N. M. Mubarak, M. Khalid, R. Walvekar, A. Numan), Springer International Publishing, Cham **2021**, pp. 319–343.
[13] W. Meng, X. Liu, H. Song, Y. Xie, X. Shi, M. Dargusch, Z.-G. Chen, Z. Tang, S. Lu, *Nano Today* **2021**, *40*, 101273.
[14] N. Khosroshahi, M. Bakhtian, A. Asadi, V. Safarifard, *Nano Express* **2023**, *4*, 042002.
[15] S. R. Jambovane, S. K. Nune, R. T. Kelly, B. P. McGrail, Z. Wang, M. I. Nandasiri, S. Katipamula, C. Trader, H. T. Schaef, *Sci. Rep.* **2016**, *6*, 36657.
[16] O. Aktas, A. C. Peacock, *Adv. Photonics Res.* **2021**, *2*, 2000159.
[17] B.-W. Su, X.-L. Zhang, W. Xin, H.-W. Guo, Y.-Z. Zhang, Z.-B. Liu, J.-G. Tian, *J. Mater. Chem. C* **2021**, *9*, 2599.
[18] T. Yang, H. Lin, B. Jia, *Front. Optoelectron.* **2018**, *11*, 2.
[19] A. Lipovka, I. Petrov, M. Fatkullin, G. Murastov, A. Ivanov, N. E. Villa, S. Shchadenko, A. Averkiev, A. Chernova, F. Gubarev, M. Saqib, W. Sheng, J.-J. Chen, O. Kanoun, I. Amin, R. D. Rodriguez, E. Sheremet, *Carbon N. Y.* **2022**, *194*, 154.
[20] R. D. Rodriguez, S. Shchadenko, G. Murastov, A. Lipovka, M. Fatkullin, I. Petrov, T.-H. Tran, A. Khalelov, M. Saqib, N. E. Villa, V. Bogoslovskiy, Y. Wang, C.-G. Hu, A. Zinovyev, W. Sheng, J.-J. Chen, I. Amin, E. Sheremet, *Adv. Funct. Mater.* **2021**, *31*, 2008818.
[21] R. D. Rodriguez, G. V. Murastov, A. Lipovka, M. I. Fatkullin, O. Nozdrina, S. K. Pavlov, P. S. Postnikov, M. M. Chehimi, J.-J. Chen, E. Sheremet, *Carbon N. Y.* **2019**, *151*, 148.
[22] A. Ren, J. Zou, H. Lai, Y. Huang, L. Yuan, H. Xu, K. Shen, H. Wang, S. Wei, Y. Wang, X. Hao, J. Zhang, D. Zhao, J. Wu, Z. Wang, *Mater. Horiz.* **2020**, *7*, 1901.
[23] N. D. Scarisoreanu, F. Craciun, M. Dinescu, V. Ion, A. Andrei, A. Moldovan, V. Teodorescu, C. Ghica, R. Birjega, in *Functional Nanostructured Interfaces for Environmental and Biomedical Applications*, Elsevier, Amsterdam **2019**, pp. 113–152.
[24] Y. Yuan, L. Jiang, X. Li, P. Zuo, X. Zhang, Y. Lian, Y. Ma, M. Liang, Y. Zhao, L. Qu, *Adv. Mater.* **2022**, *34*, 2110013.
[25] J. Yan, H. Li, M. H. Aldamasy, C. Frasca, A. Abate, K. Zhao, Y. Hu, *Chem. Mater.* **2023**, *35*, 2683.
[26] M.-A. Gatou, I.-A. Vagena, N. Lagopati, N. Pippa, M. Gazouli, E. A. Pavlatou, *Nanomaterials (Basel)* **2023**, *13*, 2224.
[27] A. Kojima, K. Teshima, Y. Shirai, T. Miyasaka, *J. Am. Chem. Soc.* **2009**, *131*, 6050.
[28] C. Li, L. Zhang, J. Chen, X. Li, J. Sun, J. Zhu, X. Wang, Y. Fu, *Nanoscale* **2021**, *13*, 485.
[29] Y. Gogotsi, B. Anasori, *ACS Nano* **2019**, *13*, 8491.
[30] S. Gulati, S. Vijayan, S. K. Mansi, B. Harikumar, M. Trivedi, R. S. Varma, *Coord. Chem. Rev.* **2023**, *474*, 214853.
[31] M. H. Kumar, N. Yantara, S. Dharani, M. Graetzel, S. Mhaisalkar, P. P. Boix, N. Mathews, *Chem. Commun.* **2013**, *49*, 11089.
[32] S. Park, W. J. Chang, C. W. Lee, S. Park, H.-Y. Ahn, K. T. Nam, *Nat. Energy* **2016**, *2*, 16185.
[33] Y.-Y. Peng, B. Akuzum, N. Kurra, M.-Q. Zhao, M. Alhabeb, B. Anasori, E. C. Kumbur, H. N. Alshareef, M.-D. Ger, Y. Gogotsi, *Energy Environ. Sci.* **2016**, *9*, 2847.
[34] S. Wang, Y.-L. Du, W.-H. Liao, *Chin. Phys. B* **2017**, *26*, 017806.
[35] W. Deng, H. Huang, H. Jin, W. Li, X. Chu, D. Xiong, W. Yan, F. Chun, M. Xie, C. Luo, L. Jin, C. Liu, H. Zhang, W. Deng, W. Yang, *Adv. Opt. Mater.* **2019**, *7*, 1801521.
[36] S. Lee, E. H. Kim, S. Yu, H. Kim, C. Park, T. H. Park, H. Han, S. W. Lee, S. Baek, W. Jin, C. M. Koo, C. Park, *Adv. Funct. Mater.* **2020**, *30*, 2001224.
[37] A. Agresti, A. Pazniak, S. Pescetelli, A. Di Vito, D. Rossi, A. Pecchia, M. Auf der Maur, A. Liedl, R. Larciprete, D. V. Kuznetsov, D. Saranin, A. Di Carlo, *Nat. Mater.* **2019**, *18*, 1228.
[38] H. Jiang, S. Jin, C. Wang, R. Ma, Y. Song, M. Gao, X. Liu, A. Shen, G. J. Cheng, H. Deng, *J. Am. Chem. Soc.* **2019**, *141*, 5481.
[39] A. Levitt, D. Hegh, P. Phillips, S. Uzun, M. Anayee, J. M. Razal, Y. Gogotsi, G. Dion, *Mater. Today* **2020**, *34*, 17.
[40] A. Al-Ashouri, E. Köhnen, B. Li, A. Magomedov, H. Hempel, P. Caprioglio, J. A. Márquez, A. B. Morales Vilches, E. Kasparavicius, J. A. Smith, N. Phung, D. Menzel, M. Grischek, L. Kegelmann, D. Skroblin, C. Gollwitzer, T. Malinauskas, M. Jošt, G. Matič, B. Rech, R. Schlatmann, M. Topič, L. Korte, A. Abate, B. Stannowski, D. Neher, M. Stolterfoht, T. Unold, V. Getautis, S. Albrecht, *Science* **2020**, *370*, 1300.

[41] X. Yang, J. Yi, T. Wang, Y. Feng, J. Wang, J. Yu, F. Zhang, Z. Jiang, Z. Lv, H. Li, T. Huang, D. Si, X. Wang, R. Cao, X. Chen, *Adv. Mater.* **2022**, *34*, 2201768.
[42] I. Hussain, U. Amara, F. Bibi, A. Hanan, M. N. Lakhan, I. A. Soomro, A. Khan, I. Shaheen, U. Sajjad, G. Mohana Rani, M. S. Javed, K. Khan, M. B. Hanif, M. A. Assiri, S. Sahoo, W. Al Zoubi, D. Mohapatra, K. Zhang, *Adv. Colloid Interface Sci.* **2024**, *324*, 103077.
[43] L. Li, Y. Wang, X. Wang, R. Lin, X. Luo, Z. Liu, K. Zhou, S. Xiong, Q. Bao, G. Chen, Y. Tian, Y. Deng, K. Xiao, J. Wu, M. I. Saidaminov, H. Lin, C.-Q. Ma, Z. Zhao, Y. Wu, L. Zhang, H. Tan, *Nat. Energy* **2022**, *7*, 708.
[44] E. Aydin, T. G. Allen, M. De Bastiani, A. Razzaq, L. Xu, E. Ugur, J. Liu, S. De Wolf, *Science* **2024**, *383*, adh3849.
[45] M. Naguib, M. Kurtoglu, V. Presser, J. Lu, J. Niu, M. Heon, L. Hultman, Y. Gogotsi, M. W. Barsoum, *Adv. Mater.* **2011**, *23*, 4207.
[46] H. Kim, Z. Wang, H. N. Alshareef, *Nano Energy* **2019**, *60*, 179.
[47] F. Shahzad, A. Iqbal, H. Kim, C. M. Koo, *Adv. Mater.* **2020**, *32*, 2002159.
[48] X. Wang, L. Bannenberg, *MRS Bull.* **2021**, *46*, 755.
[49] H. Kim, H. N. Alshareef, *ACS Mater. Lett.* **2020**, *2*, 55.
[50] A. VahidMohammadi, J. Rosen, Y. Gogotsi, *Science* **2021**, *372*, abf1581.
[51] D. B. Velusamy, J. K. El-Demellawi, A. M. El-Zohry, A. Giugni, S. Lopatin, M. N. Hedhili, A. E. Mansour, E. D. Fabrizio, O. F. Mohammed, H. N. Alshareef, *Adv. Mater.* **2019**, *31*, 1807658.
[52] K. Chaudhuri, Z. Wang, M. Alhabeb, K. Maleski, Y. Gogotsi, V. Shalaev, A. Boltasseva, in *2D Metal Carbides and Nitrides (MXenes)*, Springer International Publishing, Cham **2019**, pp. 327–346.
[53] J. Xu, J. Shim, J.-H. Park, S. Lee, *Adv. Funct. Mater.* **2016**, *26*, 5328.
[54] Z. Ling, C. E. Ren, M.-Q. Zhao, J. Yang, J. M. Giammarco, J. Qiu, M. W. Barsoum, Y. Gogotsi, *Proc. Natl. Acad. Sci. USA* **2014**, *111*, 16676.
[55] Y. Zheng, W. Chen, Y. Sun, C. Huang, Z. Wang, D. Zhou, *J. Colloid Interface Sci.* **2021**, *595*, 151.
[56] S. Ma, X. Fan, Y. An, D. Yang, Z. Luo, Y. Hu, N. Guo, *J. Mater. Sci.* **2019**, *54*, 11378.
[57] M. Safaei, M. M. Foroughi, N. Ebrahimpoor, S. Jahani, A. Omidi, M. Khatami, *Trends Anal. Chem.* **2019**, *118*, 401.
[58] Y.-R. Lee, J. Kim, W.-S. Ahn, *Korean J. Chem. Eng.* **2013**, *30*, 1667.
[59] I. M. Hönicke, I. Senkovska, V. Bon, I. A. Baburin, N. Bönisch, S. Raschke, J. D. Evans, S. Kaskel, *Angew. Chem., Int. Ed.* **2018**, *57*, 13780.
[60] J.-W. Yoon, J.-H. Kim, C. Kim, H. W. Jang, J.-H. Lee, *Adv. Energy Mater.* **2021**, *11*, 2003052.
[61] S. K. Bhardwaj, N. Bhardwaj, R. Kaur, J. Mehta, A. L. Sharma, K.-H. Kim, A. Deep, *J. Mater. Chem. A* **2018**, *6*, 14992.
[62] X. Ren, G. Liao, Z. Li, H. Qiao, Y. Zhang, X. Yu, B. Wang, H. Tan, L. Shi, X. Qi, H. Zhang, *Coord. Chem. Rev.* **2021**, *435*, 213781.
[63] V. Stavila, A. A. Talin, M. D. Allendorf, *Chem. Soc. Rev.* **2014**, *43*, 5994.
[64] J. G. Santaclara, F. Kapteijn, J. Gascon, M. A. van der Veen, *CrystEngComm* **2017**, *19*, 4118.
[65] Z. Li, G. Wang, Y. Ye, B. Li, H. Li, B. Chen, *Angew. Chem.* **2019**, *131*, 18193.
[66] J. Yan, T. Liu, X. Liu, Y. Yan, Y. Huang, *Coord. Chem. Rev.* **2022**, *452*, 214300.
[67] S. Zhang, J. Wang, Y. Zhang, J. Ma, L. Huang, S. Yu, L. Chen, G. Song, M. Qiu, X. Wang, *Environ. Pollut.* **2021**, *291*, 118076.
[68] Y. Zheng, F.-Z. Sun, X. Han, J. Xu, X.-H. Bu, *Adv. Opt. Mater.* **2020**, *8*, 2000110.
[69] A. E. Baumann, D. A. Burns, B. Liu, V. S. Thoi, *Commun. Chem.* **2019**, *2*, 86.
[70] J. H. Lee, S. Jeoung, Y. G. Chung, H. R. Moon, *Coord. Chem. Rev.* **2019**, *389*, 161.
[71] L. S. Xie, G. Skorupskii, M. Dincă, *Chem. Rev.* **2020**, *120*, 8536.
[72] Q. Liang, S. Cui, C. Liu, S. Xu, C. Yao, Z. Li, *J. Colloid Interface Sci.* **2018**, *524*, 379.
[73] K. T. Butler, C. H. Hendon, A. Walsh, *J. Am. Chem. Soc.* **2014**, *136*, 2703.
[74] X. Guo, L. Liu, Y. Xiao, Y. Qi, C. Duan, F. Zhang, *Coord. Chem. Rev.* **2021**, *435*, 213785.
[75] J. Jagielski, S. Kumar, W.-Y. Yu, C.-J. Shih, *J. Mater. Chem. C* **2017**, *5*, 5610.
[76] J. Ma, H. Wang, D. Li, *Adv. Mater.* **2021**, *33*, 2008785.
[77] L. Chouhan, S. Ghimire, C. Subrahmanyam, T. Miyasaka, V. Biju, *Chem. Soc. Rev.* **2020**, *49*, 2869.
[78] L. N. Quan, B. P. Rand, R. H. Friend, S. G. Mhaisalkar, T.-W. Lee, E. H. Sargent, *Chem. Rev.* **2019**, *119*, 7444.
[79] J. W. Bennett, I. Grinberg, A. M. Rappe, *Phys. Rev. B* **2009**, *79*, 235115.
[80] Y. Liao, H. Liu, W. Zhou, D. Yang, Y. Shang, Z. Shi, B. Li, X. Jiang, L. Zhang, L. N. Quan, R. Quintero-Bermudez, B. R. Sutherland, Q. Mi, E. H. Sargent, Z. Ning, *J. Am. Chem. Soc.* **2017**, *139*, 6693.
[81] X. Du, G. Wu, J. Cheng, H. Dang, K. Ma, Y.-W. Zhang, P.-F. Tan, S. Chen, *RSC Adv.* **2017**, *7*, 10391.
[82] S. Rhee, K. An, K.-T. Kang, *Crystals (Basel)* **2020**, *11*, 39.
[83] A. Fakharuddin, U. Shabbir, W. Qiu, T. Iqbal, M. Sultan, P. Heremans, L. Schmidt-Mende, *Adv. Mater.* **2019**, *31*, 1807095.
[84] J. Huang, S. Tan, P. D. Lund, H. Zhou, *Energy Environ. Sci.* **2017**, *10*, 2284.
[85] Y.-H. Kim, H. Cho, J. H. Heo, T.-S. Kim, N. Myoung, C.-L. Lee, S. H. Im, T.-W. Lee, *Adv. Mater.* **2015**, *27*, 1248.
[86] M. A. Green, A. Ho-Baillie, H. J. Snaith, *Nat. Photonics* **2014**, *8*, 506.
[87] N. Ilyas, J. Wang, C. Li, D. Li, H. Fu, D. Gu, X. Jiang, F. Liu, Y. Jiang, W. Li, *Adv. Funct. Mater.* **2022**, *32*, 2110976.
[88] A decade of perovskite photovoltaics, *Nat. Energy* **2019**, *4*, 1.
[89] Z. Li, T. R. Klein, D. H. Kim, M. Yang, J. J. Berry, M. F. A. M. van Hest, K. Zhu, *Nat. Rev. Mater.* **2018**, *3*, 18017.
[90] T. Ava, A. Al Mamun, S. Marsillac, G. Namkoong, *Appl. Sci.* **2019**, *9*, 188.
[91] A. Fakharuddin, M. K. Gangishetty, M. Abdi-Jalebi, S.-H. Chin, A. R. bin Mohd Yusoff, D. N. Congreve, W. Tress, F. Deschler, M. Vasilopoulou, H. J. Bolink, *Nat. Electron.* **2022**, *5*, 203.
[92] S. Tao, I. Schmidt, G. Brocks, J. Jiang, I. Tranca, K. Meerholz, S. Olthof, *Nat. Commun.* **2019**, *10*, 2560.
[93] D. Saranin, S. Pescetelli, A. Pazniak, D. Rossi, A. Liedl, A. Yakusheva, L. Luchnikov, D. Podgorny, P. Gostischev, S. Didenko, A. Tameev, D. Lizzit, M. Angelucci, R. Cimino, R. Larciprete, A. Agresti, A. Di Carlo, *Nano Energy* **2021**, *82*, 105771.
[94] A. Di Vito, A. Pecchia, M. Auf der Maur, A. Di Carlo, *Adv. Funct. Mater.* **2020**, *30*, 1909028.
[95] C. Wu, W. Fang, Q. Cheng, J. Wan, R. Wen, Y. Wang, Y. Song, M. Li, *Angew. Chem., Int Ed Engl.* **2022**, *61*, 202210970.
[96] M. R. Khan, T. W. Chuan, A. Yousuf, M. N. K. Chowdhury, C. K. Cheng, *Catal. Sci. Technol.* **2015**, *5*, 2522.
[97] E. M. Sharaf Aldeen, A. A. Jalil, R. S. Mim, A. H. Hatta, N. I. H. Hazril, A. Chowdhury, N. S. Hassan, S. Rajendran, *Environ. Res.* **2023**, *234*, 116576.
[98] K. Saravanakumar, K. Yun, V. Maheskumar, Y. Yea, G. Jagan, C. M. Park, *Chem. Eng. J.* **2023**, *451*, 138933.
[99] J. Ren, T. Li, X. Zhou, X. Dong, A. V. Shorokhov, M. B. Semenov, V. D. Krevchik, Y. Wang, *Chem. Eng. J.* **2019**, *358*, 30.
[100] C. Zhang, W. Li, L. Li, *Angew. Chem.* **2021**, *133*, 7564.
[101] A. V. Vinogradov, H. Zaake-Hertling, E. Hey-Hawkins, A. V. Agafonov, G. A. Seisenbaeva, V. G. Kessler, V. V. Vinogradov, *Chem. Commun.* **2014**, *50*, 10210.
[102] X. Hou, L. Pan, S. Huang, O.-Y. Wei, X. Chen, *Electrochim. Acta* **2017**, *236*, 351.
[103] B. Li, J. Zhao, Q. Lu, S. Zhou, H. Wei, T. Lv, Y. Zhang, J. Zhang, Q. Liu, *Energy Technol.* **2021**, *9*, 2000957.

[104] C.-C. Chueh, C.-I. Chen, Y.-A. Su, H. Konnerth, Y.-J. Gu, C.-W. Kung, K. C.-W. Wu, *J. Mater. Chem. A* **2019**, *7*, 17079.
[105] H.-Y. Chung, C.-H. Lin, S. Prabu, H.-W. Wang, *J. Chin. Chem. Soc.* **2018**, *65*, 1476.
[106] H. Zong, R. Qi, K. Yu, Z. Zhu, *Electrochim. Acta* **2021**, *393*, 139068.
[107] X. Fu, L. Zhao, Z. Yuan, Y. Zheng, V. Shulga, W. Han, L. Wang, *Adv. Mater. Technol.* **2022**, *7*, 2101511.
[108] Y. Wang, J. Song, W.-Y. Wong, *Angew. Chem.* **2023**, *135*, 202218343.
[109] L.-Y. Wu, Y.-F. Mu, X.-X. Guo, W. Zhang, Z.-M. Zhang, M. Zhang, T.-B. Lu, *Angew. Chem., Int. Ed Engl.* **2019**, *58*, 9491.
[110] M. Chamack, M. Ifires, S. A. Akbar Razavi, A. Morsali, A. Addad, A. Larimi, S. Szunerits, R. Boukherroub, *Inorg. Chem.* **2022**, *61*, 1735.
[111] Y. Wu, X. Li, Q. Yang, D. Wang, F. Yao, J. Cao, Z. Chen, X. Huang, Y. Yang, X. Li, *Chem. Eng. J.* **2020**, *390*, 124519.
[112] H. Shahriyari Far, M. Najafi, M. Hasanzadeh, R. Rahimi, *Inorg. Chem. Commun.* **2023**, *152*, 110680.
[113] C. Cheng, J. Zhang, B. Zhu, G. Liang, L. Zhang, J. Yu, *Angew. Chem.* **2023**, *135*, 202218688.
[114] P. Urbankowski, B. Anasori, K. Hantanasirisakul, L. Yang, L. Zhang, B. Haines, S. J. May, S. J. L. Billinge, Y. Gogotsi, *Nanoscale* **2017**, *9*, 17722.
[115] H. Tang, R. Wang, L. Shi, E. Sheremet, R. D. Rodriguez, J. Sun, *Chem. Eng. J.* **2021**, *425*, 131472.
[116] J. L. Hart, K. Hantanasirisakul, A. C. Lang, B. Anasori, D. Pinto, Y. Pivak, J. T. van Omme, S. J. May, Y. Gogotsi, M. L. Taheri, *Nat. Commun.* **2019**, *10*, 522.
[117] L. Liu, H. Zschiesche, M. Antonietti, B. Daffos, N. V. Tarakina, M. Gibilaro, P. Chamelot, L. Massot, B. Duployer, P. Taberna, P. Simon, *Adv. Energy Mater.* **2023**, *13*, 2202709.
[118] B. Ji, S. Fan, X. Ma, K. Hu, L. Wang, C. Luan, J. Deng, L. Cheng, L. Zhang, *Carbon N. Y.* **2020**, *165*, 150.
[119] R. Liu, M. Miao, Y. Li, J. Zhang, S. Cao, X. Feng, *ACS Appl. Mater. Interfaces* **2018**, *10*, 44787.
[120] X. Wu, Z. Wang, M. Yu, L. Xiu, J. Qiu, *Adv. Mater.* **2017**, *29*, 1607017.
[121] P. O. Å. Persson, J. Rosen, *Curr. Opin. Solid State Mater. Sci.* **2019**, *23*, 100774.
[122] M. Khazaei, A. Mishra, N. S. Venkataramanan, A. K. Singh, S. Yunoki, *Curr. Opin. Solid State Mater. Sci.* **2019**, *23*, 164.
[123] J. Jiang, S. Bai, J. Zou, S. Liu, J.-P. Hsu, N. Li, G. Zhu, Z. Zhuang, Q. Kang, Y. Zhang, *Nano Res.* **2022**, *15*, 6551.
[124] M. Naguib, M. W. Barsoum, Y. Gogotsi, *Adv. Mater.* **2021**, *33*, 2103393.
[125] N. Goel, A. Kushwaha, M. Kumar, *RSC Adv.* **2022**, *12*, 25172.
[126] J. E. Mondloch, O. Karagiaridi, O. K. Farha, J. T. Hupp, *CrystEngComm* **2013**, *15*, 9258.
[127] Y. Yoo, V. Varela-Guerrero, H.-K. Jeong, *Langmuir* **2011**, *27*, 2652.
[128] E. S. Sanil, K.-H. Cho, D.-Y. Hong, J. S. Lee, S.-K. Lee, S. G. Ryu, H. W. Lee, J.-S. Chang, Y. K. Hwang, *Chem. Commun.* **2015**, *51*, 8418.
[129] H. Meng, Y. Han, C. Zhou, Q. Jiang, X. Shi, C. Zhan, R. Zhang, *Small Methods* **2020**, *4*, 2000396.
[130] Y. Zhao, Z. Song, X. Li, Q. Sun, N. Cheng, S. Lawes, X. Sun, *Energy Storage Mater.* **2016**, *2*, 35.
[131] D. Li, H.-Q. Xu, L. Jiao, H.-L. Jiang, *EnergyChem* **2019**, *1*, 100005.
[132] R.-B. Lin, S. Xiang, H. Xing, W. Zhou, B. Chen, *Coord. Chem. Rev.* **2019**, *378*, 87.
[133] M. Ding, X. Cai, H.-L. Jiang, *Chem. Sci.* **2019**, *10*, 10209.
[134] Y. I. Lee, N. J. Jeon, B. J. Kim, H. Shim, T.-Y. Yang, S. I. Seok, J. Seo, S. G. Im, *Adv. Energy Mater.* **2018**, *8*, 1701928.
[135] F. Zhang, K. Zhu, *Adv. Energy Mater.* **2020**, *10*, 1902579.
[136] C. F. Arias-Ramos, Y. Kumar, P. G. Abrego-Martínez, H. Hu, *Sol. Energy Mater. Sol. Cells* **2020**, *215*, 110625.
[137] J. C. Yu, D. W. Kim, D. B. Kim, E. D. Jung, J. H. Park, A.-Y. Lee, B. R. Lee, D. Di Nuzzo, R. H. Friend, M. H. Song, *Adv. Mater.* **2016**, *28*, 6906.
[138] V. L. Pool, B. Dou, D. G. Van Campen, T. R. Klein-Stockert, F. S. Barnes, S. E. Shaheen, M. I. Ahmad, M. F. A. M. van Hest, M. F. Toney, *Nat. Commun.* **2017**, *8*, 14075.
[139] B. Wang, S. Bi, J. Zhou, N. Ahmad, D. Zhang, Y. Zhang, H. Zhou, *J. Mater. Chem. C* **2021**, *9*, 14749.
[140] V. G. V. Dutt, V. G. Vasavi Dutt, S. Akhil, N. Mishra, *ChemNanoMat* **2020**, *6*, 1730.
[141] K. P. Marshall, M. Walker, R. I. Walton, R. A. Hatton, *Nat. Energy* **2016**, *1*, 16178.
[142] Z. Fang, M. Shang, X. Hou, Y. Zheng, Z. Du, Z. Yang, K.-C. Chou, W. Yang, Z. L. Wang, Y. Yang, *Nano Energy* **2019**, *61*, 389.
[143] D. Bai, J. Zhang, Z. Jin, H. Bian, K. Wang, H. Wang, L. Liang, Q. Wang, S. F. Liu, *ACS Energy Lett.* **2018**, *3*, 970.
[144] Y. Zhao, Y. Wang, J. Duan, X. Yang, Q. Tang, *J. Mater. Chem. A* **2019**, *7*, 6877.
[145] Y. Hu, F. Bai, X. Liu, Q. Ji, X. Miao, T. Qiu, S. Zhang, *ACS Energy Lett.* **2017**, *2*, 2219.
[146] J. Jiang, Q. Wang, Z. Jin, X. Zhang, J. Lei, H. Bin, Z.-G. Zhang, Y. Li, S. F. Liu, *Adv. Energy Mater.* **2018**, *8*, 1701757.
[147] G. Wang, M. Lei, J. Liu, Q. He, W. Zhang, *Sol. RRL* **2020**, *4*, 2000528.
[148] J. Xue, R. Wang, Y. Yang, *Nat. Rev. Mater.* **2020**, *5*, 809.
[149] P. Docampo, T. Bein, *Acc. Chem. Res.* **2016**, *49*, 339.
[150] Y. Rong, Y. Hu, A. Mei, H. Tan, M. I. Saidaminov, S. I. Seok, M. D. McGehee, E. H. Sargent, H. Han, *Science* **2018**, *361*, aat8235.
[151] N. Li, X. Niu, L. Li, H. Wang, Z. Huang, Y. Zhang, Y. Chen, X. Zhang, C. Zhu, H. Zai, Y. Bai, S. Ma, H. Liu, X. Liu, Z. Guo, G. Liu, R. Fan, H. Chen, J. Wang, Y. Lun, X. Wang, J. Hong, H. Xie, D. S. Jakob, X. G. Xu, Q. Chen, H. Zhou, *Science* **2021**, *373*, 561.
[152] R. Kumar, A. Pérez del Pino, S. Sahoo, R. K. Singh, W. K. Tan, K. K. Kar, A. Matsuda, E. Joanni, *Prog. Energy Combust. Sci.* **2022**, *91*, 100981.
[153] S. Hong, H. Lee, J. Yeo, S. H. Ko, *Nano Today* **2016**, *11*, 547.
[154] H. Liu, Z. Sun, Y. Chen, W. Zhang, X. Chen, C.-P. Wong, *ACS Nano* **2022**, *16*, 10088.
[155] M. S. Brown, C. B. Arnold, in *Laser Precision Microfabrication*, Springer, Berlin, Heidelberg **2010**, pp. 91–120.
[156] A. Hu, Y. Zhou, W. W. Duley, *Open Surf. Sci. J.* **2010**, *3*, 42.
[157] E. Greenberg, N. Armon, O. Kapon, M. Ben-Ishai, H. Shpaisman, *Adv. Mater. Interfaces* **2019**, *6*, 1900541.
[158] N. Hartmann, T. Balgar, R. Bautista, S. Franzka, *Surf. Sci.* **2006**, *600*, 4034.
[159] D. Bäuerle, *Laser Processing and Chemistry*, Springer, Berlin, Heidelberg **1996**.
[160] A. Royon, Y. Petit, G. Papon, M. Richardson, L. Canioni, *Opt. Mater. Express* **2011**, *1*, 866.
[161] D. Rayner, A. Naumov, P. Corkum, *Opt. Express* **2005**, *13*, 3208.
[162] J. Theerthagiri, K. Karuppasamy, S. J. Lee, R. Shwetharani, H.-S. Kim, S. K. K. Pasha, M. Ashokkumar, M. Y. Choi, *Light: Sci. Appl.* **2022**, *11*, 250.
[163] H. Palneedi, J. H. Park, D. Maurya, M. Peddigari, G.-T. Hwang, V. Annapureddy, J.-W. Kim, J.-J. Choi, B.-D. Hahn, S. Priya, K. J. Lee, J. Ryu, *Adv. Mater.* **2018**, *30*, 1705148.
[164] M. Xiao, S. Zheng, D. Shen, W. W. Duley, Y. N. Zhou, *Nano Today* **2020**, *35*, 100959.
[165] Y.-J. Tang, H. Zheng, Y. Wang, W. Zhang, K. Zhou, *Adv. Funct. Mater.* **2021**, *31*, 2102648.
[166] C. T. Lee, S. W. Han, M. W. Shin, *Surf. Interfaces* **2022**, *30*, 101904.
[167] S. Malyukov, A. Sayenko, Y. Klunnikova, presented at 2018 Int. Russian Automation Conf. (RusAutoCon), Sochi, Russia, September **2018**.
[168] P. You, G. Li, G. Tang, J. Cao, F. Yan, *Energy Environ. Sci.* **2020**, *13*, 1187.
[169] Y. Zhang, L. Wang, L. Zhao, K. Wang, Y. Zheng, Z. Yuan, D. Wang, X. Fu, G. Shen, W. Han, *Adv. Mater.* **2021**, *33*, 2007890.

[170] N. Kurra, B. Ahmed, Y. Gogotsi, H. N. Alshareef, *Adv. Energy Mater.* **2016**, *6*, 1601372.
[171] X. Li, Y. Ma, P. Shen, C. Zhang, J. Yan, Y. Xia, S. Luo, Y. Gao, *ChemElectroChem* **2020**, *7*, 821.
[172] H. Li, Y. Liu, S. Lin, H. Li, Z. Wu, L. Zhu, C. Li, X. Wang, X. Zhu, Y. Sun, *J. Power Sources* **2021**, *497*, 229882.
[173] J. Tang, W. Yi, X. Zhong, C. J. Zhang, X. Xiao, F. Pan, B. Xu, *Energy Storage Mater.* **2020**, *32*, 418.
[174] J. Zhao, J. Gao, Z. Zhou, J. Gui, Y. Wang, X. Wu, M. Li, R. Xu, *IEEE Sens. J.* **2021**, *21*, 26673.
[175] C. Zhang, J. Chen, J. Gao, G. Tan, S. Bai, K. Weng, H. M. Chen, X. Ding, H. Cheng, Y. Yang, J. Wang, *Nano Lett.* **2023**, *23*, 3435.
[176] M. Sharifuzzaman, M. A. Zahed, S. Sharma, S. Yoon, C. Park, J. Y. Park, presented at 2021 21st International Conference on Solid-State Sensors, Actuators and Microsystems (Transducers), Orlando, FL, USA, June **2021**.
[177] M. Sharifuzzaman, M. A. Zahed, M. S. Reza, M. Asaduzzaman, S. Jeong, H. Song, D. K. Kim, S. Zhang, J. Y. Park, *Adv. Funct. Mater.* **2023**, *33*, 2208894.
[178] W. Zhang, R. Li, H. Zheng, J. Bao, Y. Tang, K. Zhou, *Adv. Funct. Mater.* **2021**, *31*, 2009057.
[179] A. Basu, K. Roy, N. Sharma, S. Nandi, R. Vaidhyanathan, S. Rane, C. Rode, S. Ogale, *ACS Appl. Mater. Interfaces* **2016**, *8*, 31841.
[180] D. Kogolev, O. Semyonov, N. Metalnikova, M. Fatkullin, R. D. Rodriguez, P. Slepicka, Y. Yamauchi, O. Guselnikova, R. Boukherroub, P. S. Postnikov, *J. Mater. Chem. A* **2023**, *11*, 1108.
[181] M. Salauddin, S. M. S. Rana, M. Sharifuzzaman, S. H. Lee, M. A. Zahed, Y. Do Shin, S. Seonu, H. S. Song, T. Bhatta, J. Y. Park, *Nano Energy* **2022**, *100*, 107462.
[182] K. Hirai, K. Sada, *Chem. Commun.* **2017**, *53*, 5275.
[183] Y. Liu, N. Chai, X. Wang, Z. Luo, J. Zhao, C. Xie, Z. Gan, *Opt. Express* **2021**, *29*, 39304.
[184] R. Ma, H. Jiang, C. Wang, C. Zhao, H. Deng, *Chem. Commun.* **2020**, *56*, 2715.
[185] K.-Y. Wang, L. Feng, T.-H. Yan, S. Wu, E. A. Joseph, H.-C. Zhou, *Angew. Chem.* **2020**, *132*, 11445.
[186] X. Huang, Q. Guo, D. Yang, X. Xiao, X. Liu, Z. Xia, F. Fan, J. Qiu, G. Dong, *Nat. Photonics* **2019**, *14*, 82.
[187] X. Xu, Y. Dong, Y. Zhang, Z. Han, J. Liu, D. Yu, Y. Wei, Y. Zou, B. Huang, J. Chen, H. Zeng, *Nano Res.* **2022**, *15*, 5476.
[188] P. K. Kanaujia, G. Vijaya Prakash, *Phys. Chem. Chem. Phys.* **2016**, *18*, 9666.
[189] Q. Li, Q. Wang, L. Li, L. Yang, Y. Wang, X. Wang, H.-T. Fang, *Adv. Energy Mater.* **2020**, *10*, 2000470.
[190] C. Xiong, Z. Wang, X. Peng, Y. Guo, S. Xu, T. Zhao, *J. Mater. Chem. A* **2020**, *8*, 14114.
[191] X. Chen, S. Wang, J. Shi, X. Du, Q. Cheng, R. Xue, Q. Wang, M. Wang, L. Ruan, W. Zeng, *Adv. Mater. Interfaces* **2019**, *6*, 1901160.
[192] X. Zang, C. Jian, T. Zhu, Z. Fan, W. Wang, M. Wei, B. Li, M. Follmar Diaz, P. Ashby, Z. Lu, Y. Chu, Z. Wang, X. Ding, Y. Xie, J. Chen, J. N. Hohman, M. Sanghadasa, J. C. Grossman, L. Lin, *Nat. Commun.* **2019**, *10*, 3112.
[193] R. Bo, M. Taheri, H. Chen, J. Bradford, N. Motta, S. Surve, T. Tran-Phu, P. Garg, T. Tsuzuki, P. Falcaro, A. Tricoli, *Adv. Funct. Mater.* **2022**, *32*, 2100351.
[194] M. Navarro, B. Seoane, E. Mateo, R. Lahoz, G. F. de la Fuente, J. Coronas, *J. Mater. Chem. A* **2014**, *2*, 11177.
[195] E. L. Ribeiro, S. A. Davari, S. Hu, D. Mukherjee, B. Khomami, *Mater. Chem. Front.* **2019**, *3*, 1302.
[196] S. L. Campello, G. Gentil, S. A. Júnior, W. M. de Azevedo, *Mater. Lett.* **2015**, *148*, 200.
[197] F. Ataei, D. Dorranian, N. Motakef-Kazemi, *J. Theor. Appl. Phys.* **2020**, *14*, 1.
[198] B. Turan, A. Huuskonen, I. Kühn, T. Kirchartz, S. Haas, *Sol. RRL* **2017**, *1*, 1700003.
[199] C. Schultz, M. Fenske, J. Dagar, A. Zeiser, A. Bartelt, R. Schlatmann, E. Unger, B. Stegemann, *Sol. Energy* **2020**, *198*, 410.
[200] L. Bayer, X. Ye, P. Lorenz, K. Zimmer, *Appl. Phys. A: Mater. Sci. Process.* **2017**, *123*, 619.
[201] X. Zheng, *J. Alloys Compd.* **2022**, *899*, 163275.
[202] N. Wang, J. Liu, Y. Zhao, M. Hu, R. Qin, G. Shan, *ChemNanoMat* **2019**, *5*, 658.
[203] W. Zhou, Z. Zhou, S. Guo, Y. Fan, N. Nomura, *Compos. Commun.* **2022**, *29*, 101034.
[204] L. An, X. Liu, B. Deng, H. Jiang, G. J. Cheng, *Matter* **2021**, *4*, 3977.
[205] S. Guo, Y. Zhao, H. Yuan, C. Wang, H. Jiang, G. J. Cheng, *Small* **2020**, *16*, 2000749.
[206] D. Van Lam, D. T. Dung, J.-H. Kim, H. Kim, S.-M. Lee, *Chem. Eng. J.* **2022**, *437*, 135237.
[207] D. Fischer, A. von Mankowski, A. Ranft, S. K. Vasa, R. Linser, J. Mannhart, B. V. Lotsch, *Chem. Mater.* **2017**, *29*, 5148.
[208] F. Stock, F. Antoni, L. Diebold, C. Chowde Gowda, S. Hajjar-Garreau, D. Aubel, N. Boubiche, F. Le Normand, D. Muller, *Appl. Surf. Sci.* **2019**, *464*, 562.
[209] A. C. Badgujar, R. O. Dusane, S. R. Dhage, *Sol. Energy* **2020**, *199*, 47.
[210] F. Chiodi, R. Daubriac, S. Kerdilès, in *Laser Annealing Processes in Semiconductor Technology*, Elsevier, Amsterdam **2021**, pp. 357–400.
[211] G. Amutha, I. A. Palani, N. J. Vasa, M. Singaperumal, T. Okada, *J. Solid Mech. Mater. Eng.* **2013**, *7*, 206.
[212] S. F. Lombardo, G. Fisicaro, I. Deretzis, A. La Magna, B. Curver, B. Lespinasse, K. Huet, *Appl. Surf. Sci.* **2019**, *467–468*, 666.
[213] V. Thampy, A. Y. Fong, N. P. Calta, J. Wang, A. A. Martin, P. J. Depond, A. M. Kiss, G. Guss, Q. Xing, R. T. Ott, A. van Buuren, M. F. Toney, J. N. Weker, M. J. Kramer, M. J. Matthews, C. J. Tassone, K. H. Stone, *Sci. Rep.* **2020**, *10*, 1981.
[214] G. Williams, B. Seger, P. V. Kamat, *ACS Nano* **2008**, *2*, 1487.
[215] Y. Zhou, Q. Bao, B. Varghese, L. A. L. Tang, C. K. Tan, C.-H. Sow, K. P. Loh, *Adv. Mater.* **2010**, *22*, 67.
[216] R. Arul, R. N. Oosterbeek, J. Robertson, G. Xu, J. Jin, M. C. Simpson, *Carbon N. Y.* **2016**, *99*, 423.
[217] X. Xie, C. Zhou, X. Wei, W. Hu, Q. Ren, *Opto-Electron. Adv.* **2019**, *2*, 18001701.
[218] L. A. Dobrzański, A. Drygała, J. Mater, *Process. Technol.* **2007**, *191*, 228.
[219] N. Li, J. Peng, W.-J. Ong, T. Ma, Arramel, P. Zhang, J. Jiang, X. Yuan, C. J. Zhang, *Matter* **2021**, *4*, 377.
[220] L. V. Thekkekara, B. Jia, Y. Zhang, L. Qiu, D. Li, M. Gu, *Appl. Phys. Lett.* **2015**, *107*, 031105.
[221] X.-Y. Fu, R.-Y. Shu, C.-J. Ma, Y.-Y. Zhang, H.-B. Jiang, *ACS Appl Nano Mater.* **2023**, *6*, 4567.
[222] X.-Y. Fu, R.-Y. Shu, C.-J. Ma, Y.-Y. Zhang, H.-B. Jiang, M.-N. Yao, *Appl. Surf. Sci.* **2023**, *631*, 157549.
[223] S. Guo, M. Gao, W. Zhang, F. Liu, X. Guo, K. Zhou, *Adv. Mater.* **2023**, *35*, 2303065.
[224] G. V. Murastov, A. A. Lipovka, M. I. Fatkullin, R. D. Rodriguez, E. S. Sheremet, *Phys.–Usp.* **2022**, *193*, 1173.
[225] M. Fatkullin, R. D. Rodriguez, I. Petrov, N. E. Villa, A. Lipovka, M. Gridina, G. Murastov, A. Chernova, E. Plotnikov, A. Averkiev, D. Cheshev, O. Semyonov, F. Gubarev, K. Brazovskiy, W. Sheng, I. Amin, J. Liu, X. Jia, E. Sheremet, *Nanomaterials* **2023**, *13*, 923.
[226] J. P. Singh, S. N. Thakur, in *Laser-Induced Breakdown Spectroscopy*, Elsevier, Amsterdam **2007**, pp. 41–70.
[227] M. Hashida, H. Mishima, S. Tokita, S. Sakabe, *Opt. Express* **2009**, *17*, 13116.
[228] R. J. Levis, *Annu. Rev. Phys. Chem.* **1994**, *45*, 483.
[229] A. R. Bahramian, M. Kokabi, in *Polymer Green Flame Retardants*, Elsevier, Amsterdam **2014**, pp. 461–502.
[230] N. A. Inogamov, Y. V. Petrov, V. A. Khokhlov, V. V. Zhakhovskii, *High Temp.* **2020**, *58*, 632.

[231] S. Ravi-Kumar, B. Lies, X. Zhang, H. Lyu, H. Qin, *Polym. Int.* **2019**, *68*, 1391.

[232] L. V. Zhigilei, P. B. S. Kodali, B. J. Garrison, *J. Phys. Chem. B* **1998**, *102*, 2845.

[233] B.-Q. Lin, C.-P. Huang, K.-Y. Tian, P.-H. Lee, W.-F. Su, L. Xu, *Int. J. Precis. Eng. Manuf.-Green Technol.* **2023**, *10*, 123.

[234] R. A. Rajan, H. Tao, W. Yu, J. Yang, *Mater. Today Phys.* **2023**, *31*, 101000.

[235] W. M. Steen, J. N. Kamalu, in *Materials Processing: Theory and Practices*, Elsevier, Amsterdam **1983**, pp. 15–111.

[236] W. M. Steen, in *Laser Material Processing*, Springer London, London **2003**, pp. 107.

[237] S. Kwon, Y. Yoon, J. Ahn, H. Lim, G. Kim, J.-H. Kim, K.-B. Choi, J. Lee, *Carbon N. Y.* **2018**, *137*, 136.

[238] Y. Wang, Y. Zhao, L. Qu, *J. Mater. Chem. A Mater. Energy Sustain* **2021**, *59*, 642.

[239] P. Serra, A. Piqué, *Adv. Mater. Technol.* **2019**, *4*, 1800099.

[240] L. Yin, Y. Li, X. Yao, Y. Wang, L. Jia, Q. Liu, J. Li, Y. Li, D. He, *Nano-Micro Lett.* **2021**, *13*, 78.

[241] A. Lipovka, M. Fatkullin, S. Shchadenko, I. Petrov, A. Chernova, E. Plotnikov, V. Menzelintsev, S. Li, L. Qiu, C. Cheng, R. D. Rodriguez, E. Sheremet, *ACS Appl. Mater. Interfaces* **2023**, *15*, 38946.

[242] B. Li, Q.-B. Zhu, C. Cui, C. Liu, Z.-H. Wang, S. Feng, Y. Sun, H.-L. Zhu, X. Su, Y.-M. Zhao, H.-W. Zhang, J. Yao, S. Qiu, Q.-W. Li, X.-M. Wang, X.-H. Wang, H.-M. Cheng, D.-M. Sun, *Adv. Mater.* **2022**, *34*, 2201298.

[243] P. Guo, C. Liu, X. Li, Z. Chen, H. Zhu, L. Zhu, X. Zhang, W. Zhao, N. Jia, Q. Ye, X. Xu, R. Chen, Z. Liu, X. Fan, C. Zhi, H. Wang, *Adv. Energy Mater.* **2022**, *12*, 2202395.

[244] H. Jiang, L. Tong, H. Liu, J. Xu, S. Jin, C. Wang, X. Hu, L. Ye, H. Deng, G. J. Cheng, *Matter* **2020**, *2*, 1535.

[245] O. M. M. M. da Costa, W. M. de Azevedo, *J. Lumin.* **2016**, *170*, 648.

[246] X.-L. Trinh, N.-H. Tran, H. Seo, H.-C. Kim, *Sol. Energy* **2020**, *206*, 301.

[247] T. Jeon, H. M. Jin, S. H. Lee, J. M. Lee, H. I. Park, M. K. Kim, K. J. Lee, B. Shin, S. O. Kim, *ACS Nano* **2016**, *10*, 7907.

[248] S.-Y. Liang, Y.-F. Liu, H.-J. Zhang, Z.-K. Ji, H. Xia, *ACS Appl. Mater. Interfaces* **2022**, *14*, 46958.

[249] A. L. Palma, F. Matteocci, A. Agresti, S. Pescetelli, E. Calabro, L. Vesce, S. Christiansen, M. Schmidt, A. Di Carlo, *IEEE J. Photovoltaics* **2017**, *7*, 1674.

[250] S. Razza, S. Pescetelli, A. Agresti, A. Di Carlo, *Energies* **2021**, *14*, 1069.

[251] A. Y. Zhizhchenko, P. Tonkaev, D. Gets, A. Larin, D. Zuev, S. Starikov, E. V. Pustovalov, A. M. Zakharenko, S. A. Kulinich, S. Juodkazis, A. A. Kuchmizhak, S. V. Makarov, *Small* **2020**, *16*, 2000410.

[252] H. Tanaka, in *Handbook of Crystal Growth*, Elsevier, Amsterdam **2015**, pp. 555–604.

[253] E. Kim, J. Song, T.-E. Song, H. Kim, Y.-J. Kim, Y.-W. Oh, S. Jung, I.-S. Kang, Y. Gogotsi, H. Han, C. W. Ahn, Y. Lee, *Chem. Eng. J.* **2022**, *450*, 138456.

[254] M. Volkov, E. Willinger, D. A. Kuznetsov, C. R. Müller, A. Fedorov, P. Baum, *ACS Nano* **2021**, *15*, 14071.

[255] P. M. Kumar, A. Das, L. Seban, R. G. Nair, in *Perovskite Photovoltaics*, Elsevier, Amsterdam **2018**, pp. 231–287.

[256] H. J. Snaith, *Nat. Mater.* **2018**, *17*, 372.

[257] T. A. Berhe, W.-N. Su, C.-H. Chen, C.-J. Pan, J.-H. Cheng, H.-M. Chen, M.-C. Tsai, L.-Y. Chen, A. A. Dubale, B.-J. Hwang, *Energy Environ. Sci.* **2016**, *9*, 323.

[258] J. Dagar, S. Castro-Hermosa, M. Gasbarri, A. L. Palma, L. Cina, F. Matteocci, E. Calabrò, A. Di Carlo, T. M. Brown, *Nano Res.* **2018**, *11*, 2669.

[259] W. Zhan, L. Meng, C. Shao, X.-G. Wu, K. Shi, H. Zhong, *ACS Photonics* **2021**, *8*, 765.

[260] X. Huang, L. Li, S. Zhao, L. Tong, Z. Li, Z. Peng, R. Lin, L. Zhou, C. Peng, K.-H. Xue, L. Chen, G. J. Cheng, Z. Xiong, L. Ye, *Nano-Micro Lett.* **2022**, *14*, 174.

[261] G. Yang, J. Liu, M. Zhou, J. Bai, X. Bo, A. C. S. Sustain, *Chem. Eng.* **2020**, *8*, 11947.

[262] Y. Wu, Z. Huang, H. Jiang, C. Wang, Y. Zhou, W. Shen, H. Xu, H. Deng, *ACS Appl. Mater. Interfaces* **2019**, *11*, 44573.

[263] E. V. Gunina, N. A. Zhestkij, M. Sergeev, S. V. Bachinin, Y. A. Mezenov, N. K. Kulachenkov, M. Timofeeva, V. Ivashchenko, A. S. Timin, S. A. Shipilovskikh, A. A. Yakubova, D. I. Pavlov, A. S. Potapov, J. Gong, L. Khamkhash, T. S. Atabaev, S. Bruyere, V. A. Milichko, *ACS Appl. Mater. Interfaces* **2023**, *15*, 47541.

[264] R. Ramírez, A. Melillo, S. Osella, A. M. Asiri, H. Garcia, A. Primo, *Small Methods* **2023**, *7*, 2300063.

[265] A. M. Huerta-Flores, J. Chen, L. M. Torres-Martínez, A. Ito, E. Moctezuma, T. Goto, *Fuel* **2017**, *197*, 174.

[266] F. Andrei, I. Boerasu, R. Birjega, A. Moldovan, M. Dinescu, V. Ion, C. Mihailescu, N. D. Scarisoreanu, V. Leca, *Appl. Phys. A: Mater. Sci. Process.* **2019**, *125*, 807.

[267] Y. Mu, Z. He, K. Wang, X. Pi, S. Zhou, *iScience* **2022**, *25*, 105371.

[268] F. Temerov, Y. Baghdadi, E. Rattner, S. Eslava, *ACS Appl. Energy Mater.* **2022**, *5*, 14605.

[269] M. D. T. McDonnell, D. Arnaldo, E. Pelletier, J. A. Grant-Jacob, M. Praeger, D. Karnakis, R. W. Eason, B. Mills, *J. Intell. Manuf.* **2021**, *32*, 1471.

[270] K. Shimahara, S. Tani, H. Sakurai, Y. Kobayashi, *Commun. Eng.* **2023**, *2*, 1.

[271] H. Tercan, T. A. Khawli, U. Eppelt, C. Büscher, T. Meisen, S. Jeschke, *Prod. Eng.* **2017**, *11*, 195.

Anna Lipovka is a junior researcher and assistant at the Research School of Chemistry and Biomedical Sciences at Tomsk Polytechnic University, Tomsk, Russia. She graduated with a Master's program in optics at TPU and will defend her Ph.D. in physical chemistry. She extensively works with graphene materials and their functionalization, studying and manipulating their properties, characterization, and applications in electronics.

Aura Garcia received a Ph.D. in geological and mineralogical sciences in 2022 at Tomsk Polytechnic University (TPU) in Russia. She is currently a postdoctoral researcher in the TERS-Team scientific group at TPU. Her research interests include emerging nanomaterials, laser processing, and flexible electronics.

Elena Abyzova received her Master's degree at Tomsk Polytechnic University (TPU) in 2020 on the development of flexible, water-stable graphene-based bioelectrodes for long-term use in bioelectronics. Now, she is a Ph.D. student in the Research School of Chemistry and Biomedical Sciences of TPU. She was working in the TERS-Team group since being a bachelor student. Her research interests are focused on nanocomposites of polymers and graphene-like materials obtained by laser radiation and their biomedical applications.

Maxim Fatkullin received his Master's degree in chemical technology at Tomsk Polytechnic University (TPU) in 2021. The same year, he started his Ph.D. in solid-state physics at TPU. Currently, he is a teaching assistant and a junior researcher at the Research School of Chemistry and Biomedical Sciences. His research interests include light-matter interaction and nanomaterials and their application in flexible electronics and sensing.

Ziyang Song is pursuing a Master's degree at the Shanghai Institute of Ceramics, Chinese Academy of Sciences. His work is focused on multifunctional flexible sensors.

Yuxiang Li received his Ph.D. degree from the Shanghai Institute of Ceramics, Chinese Academy of Sciences, in 2023. His research interests include flexible and wearable electronics.

Ranran Wang received her Ph.D. degree from the Shanghai Institute of Ceramics, Chinese Academy of Sciences (SICCAS) in 2012 and was co-cultivated at the University of California, Los Angeles, for two years (2010–2012). She is now working as a professor at SICCAS, focusing on the fabrication of low-dimensional conductive materials and their application in flexible electronics.

Raul D. Rodriguez is a renowned expert in nanoscience and nanotechnology. He obtained his Ph.D. with the highest honors from Sorbonne University in Paris, France, in 2009. He specializes in nanoscale characterization and has significantly contributed to developing innovative methods in this field. Currently, he holds the position of full professor at Tomsk Polytechnic University. He leads research on flexible electronics with laser processing, including exploring plasmonic and 2D nanomaterials for cutting-edge applications in biomedicine, optoelectronics, energy, and safety domains.

Evgeniya Sheremet is a renowned professor with extensive expertise in nanomaterials. Her research delves into modifying nanomaterials and creating tools for their analysis. She has contributed numerous peer-reviewed publications to her credit and received awards for developing innovative materials for electronics. As a full professor, she has secured international project grants. Her achievements include remarkable publications in top journals and prestigious awards, including the LÓreal UNESCO award. Her dedication to her field has led to significant advancements in nanomaterial research.